UNIVERSITÀ
DI PAVIA

Dipartimento di Chimica
Direttore Prof. Mauro Freccero

Corso di Laurea Magistrale in Chimica

Metallo-porphyrinoid complexes for neurodegeneration prevention: antioxidant activity and inhibition of amyloid aggregation

Complessi metallo-porfirinoidi nella prevenzione della neurodegenerazione: attività antiossidante e inibizione dell'aggregazione amiloide

Relatore:
Prof. Simone Dell'Acqua

Correlatore:
Angelo Ferraresi

Tesi di Laurea Magistrale di
Cecilia Valle

Anno Accademico 2025/2026

Table of contents

1. Introduction

1.1. Neurodegenerative diseases 1

1.2. Role and activity of metals 3

1.3. Porphyrinoid macrocycles – Corroles 5

1.4. Porphyrinoid macrocycles – Texaphyrins 7

2. Aim of the thesis 9

3. Results and discussion 11

3.1. Synthesis and Characterization of porphyrinoid complexes 11

3.1.1. Synthesis and Characterization of FeTCPC 11

3.1.2. Synthesis and Characterization of MnTPCMe 12

3.1.3. Characterization of MnTEXCOOH 13

3.2. Reactivity studies 14

3.2.1. Peroxidase-like activity of FeTCPC 14

3.2.1.1 HPA 16

3.2.1.2 4-methylcathecol 19

3.2.2. Catalase-like activity of MnTPCMe 22

3.2.3. MnTexCOOH inhibition activity on BSA aggregation 24

3.2.4. MnTexCOOH inhibition activity on $A\beta_{40}$ aggregation 28

3.2.5. MnTexCOOH inhibition activity on $A\beta_{40}$ aggregation in *E. coli* 32

4. Materials and methods 34

4.1. Instrumentation 34

4.2. Synthesis of FeTCPC 35

4.3. Synthesis of MnTPCMe 37

4.4. Characterization of MnTexCOOH 39

4.5. Hemochromogen assay 41

4.6. Reactivity studies 42

4.6.1. Peroxidase-like activity of FeTCPC 42

4.5.1.1 HPA 42

4.5.1.2 4-methylcathecol 46

4.6.2. Catalase-like activity of MnTPCMe 51

4.6.3. MnTexCOOH inhibition activity on BSA aggregation 51

4.6.4. MnTexCOOH inhibition activity on $A\beta_{40}$ aggregation 54

4.6.5. MnTexCOOH inhibition activity on $A\beta_{40}$ aggregation in *E. coli* 55

5. Conclusions 58

6. References 60

Abstract

Le malattie neurodegenerative, come la malattia di Alzheimer (AD) e il morbo di Parkinson (PD), sono accomunate da molti fattori che ne provocano l'insorgere, pur manifestandosi con quadri clinici differenti. L'AD, in particolare, è un disturbo caratterizzato da un progressivo declino delle abilità cognitive, associato ad un disorientamento spazio-temporale. Questa classe di patologie presenta dei tratti distintivi che si possono osservare in specifiche zone cerebrali, tra cui l'accumulo di placche amiloidi e grovigli neurofibrillari, lo stress ossidativo e la neuro-infiammazione. Data la natura multifattoriale di tale categoria di malattie, lo sviluppo di una terapia efficace in grado di contrastare i diversi fenomeni che ne provocano la comparsa, risulta molto difficile. Per questa ragione, attualmente la ricerca farmacologica per l'AD si concentra maggiormente sulla regolazione della produzione non regolata di specie radicaliche libere e sull'inibizione della aggregazione irreversibile di placche di β-amiloide (Aβ). Entrambi i fenomeni sono strettamente collegati all'alterazione dell'omeostasi dei metalli all'interno dell'ambiente cerebrale che si presenta in condizioni patologiche. I metalli coinvolti sono principalmente ferro, rame e zinco, elementi essenziali per il corretto svolgimento delle funzioni neuronali.[1] Nel caso della malattia di Alzheimer, tali ioni metallici si trovano in concentrazioni maggiori rispetto a quelle fisiologiche. Il loro accumulo promuove la produzione di specie reattive all'ossigeno (ROS) e l'aggregazione di peptidi Aβ, con conseguente formazione di aggregati amiloidi. La comune conseguenza è il danneggiamento strutturale e funzionale delle principali biomolecole presenti all'interno delle cellule neuronali, come lipidi, proteine e acidi nucleici, portando nei casi più gravi alla morte neuronale. La generazione di ROS catalizzata da metalli avviene principalmente mediante le reazioni di Fenton e Haber-Weiss (Fig. 1), le quali portano alla formazione di specie altamente ossidanti come il radicale idrossile ($OH^{\bullet}$) e l'anione radicale superossido ($O_2^{\bullet-}$).[2]

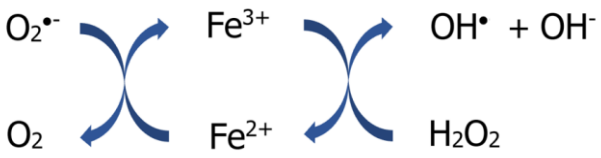

Fig. 1 *Processo Fenton/Haber-Weiss.*

In condizioni fisiologiche, l'organismo possiede sistemi di difesa antiossidante in grado di neutralizzare l'azione ossidante e dannosa delle ROS, principalmente costituiti da enzimi con attività di tipo perossidasico e catalasico. Tali enzimi catalizzano la conversione del perossido di idrogeno (nel caso delle perossidasi mediante l'ossidazione di un substrato sacrificale) con lo scopo di renderlo una specie innocua nei confronti le biomolecole presenti nelle cellule neuronali.

Il primo obbiettivo di questo studio è stato quello di individuare dei composti in grado di svolgere un'attività antiossidante nei confronti delle ROS, mediante un'azione di tipo come attività pseudo-perossidasica e pseudo-catalasica.

I composti individuati sono i corroli, macrocicli tetrapirrolici con una struttura molto simile a quella della porfirina (Fig. 2). Grazie ad una cavità del macrociclo leggermente più ristretta rispetto a quella della porfirina, i corroli sono in grado di complessare degli ioni metallici redox-attivi in alto stato di ossidazione. Pur essendo macrocicli triprotici contenenti un atomo di carbonio in meno rispetto alla porfirina, i corroli mantengono l'aromaticità dell'anello macrociclico.

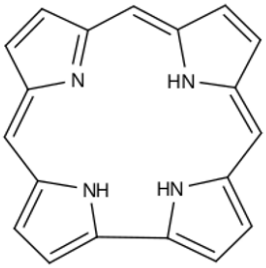

Fig. 2 *Sruttura del macrocilo corrolico.*

Con lo scopo di studiare l'attività antiossidante di tali composti, sono stati sintetizzati e caratterizzati due complessi corrolici funzionalizzati diversamente, contenenti due ioni metallici differenti (Fig. 3): Fe(IV)-5,10,15-tris(p-carbossifenil) corrolo (FeTCPC) e Mn(III)-5,10,15-tris(N-metil-4-piridil) corrolo (MnTPCMe).

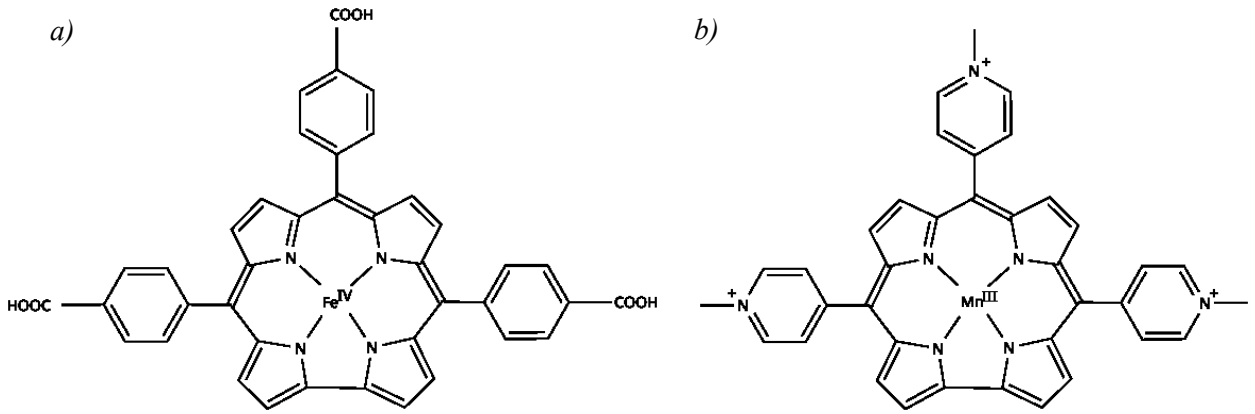

Fig. 3 *Struttura dei complessi FeTCPC (a) e MnTPCMe (b).*

Come primo step dello studio, è stata valutata l'attività pseudo-perossidasica del complesso FeTCPC, utilizzando l'emina come sistema di riferimento. La reazione catalitica di catalisi di riduzione del perossido di idrogeno coinvolge l'ossidazione di un substrato (AH) che viene convertito nella rispettiva specie radicalica. In particolare, sono stati svolti due saggi in presenza di HPA (acido 3-(4-idrossifenil) propanoico) e 4-metilcatecolo.

$$2\ AH + H_2O_2 \rightarrow 2\ A^{\bullet} + 2\ H_2O$$

Monitorando la banda di assorbimento del prodotto di ossidazione di ciascun substrato è stato possibile ricavare la velocità della reazione di ossidazione. Successivamente, sono state determinate le costanti k_{cat} e K_M mediante l'equazione di Michaelis-Menten, parametri che indicano rispettivamente della velocità con cui il substrato viene convertito in prodotto e dell'affinità apparente tra il catalizzatore e il substrato.

Dai parametri cinetici calcolati è risultato che il complesso FeTCPC mostra un valore di K_M maggiore rispetto a quello dell'emina, indice di una affinità minore verso il substrato, e un valore della k_{cat} maggiore, a dimostrazione di una maggiore velocità di turnover. Nella fase successiva dello studio è stata testata l'attività pseudo-catalasica del complesso MnTPCMe, la cui reazione catalizzata consiste nella dismutazione del perossido di idrogeno a formare una molecola di acqua e una di ossigeno.

$$2\ H_2O_2 \rightarrow 2\ H_2O + O_2$$

Per lo svolgimento dell'esperimento è stato utilizzato il substrato ABTS (acido 2,2'-azinobis[3-etilbenzotiazolino-6-solfonico), un composto che viene ossidato dall'H_2O_2 residuo nell'ambiente di reazione in presenza di un catalizzatore; osservando la diminuzione della banda di assorbimento del prodotto di ossidazione dell'ABTS, è possibile risalire indirettamente alla quantità di perossido disproporzionata dal catalizzatore. L'attività catalitica del complesso MnTPCMe è stata confrontata con quella della catalasi da fegato bovino. I risultati indicano che il complesso MnTPCMe possiede un'ottima attività pseudo-catalasica, leggermente inferiore rispetto a quella dell'enzima di riferimento.

La seconda parte dello studio, svolta presso i dipartimenti di chimica e farmacia dell'Università di Barcellona; questa sezione è stata incentrata sulla capacità di inibizione dell'aggregazione dei peptidi β-amiloidi (Aβ) a formare placche insolubili. Per questo scopo è stata utilizzata una differente categoria di composti porfirinoidi: le texafirine. Si tratta di composti macrociclici con una struttura simile a quella porfirinica, caratterizzati da una cavità coordinativa più ampia dovuta alla presenza di un quinto atomo di azoto donatore.[3] Nello specifico, è stata utilizzato il complesso manganese(II)-(9,24-idrossipropil-17-carbossil)-texapfirina (MnTexCOOH), costituito da una texafirina recante un gruppo funzionale carbossilico in cui è coordinato uno ione manganese(II) (Fig. 4). Il composto è stato fornito nell'ambito di una collaborazione con un laboratorio esterno.

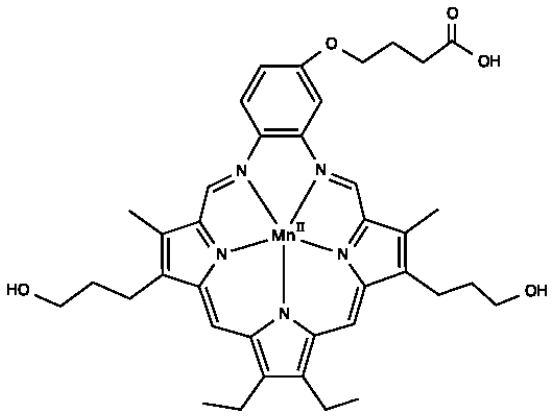

Fig. 4 *Struttura del complesso MnTexCOOH.*

I peptidi Aβ sono catene polipeptidiche costituite da 40-42 amminoacidi, caratterizzate da sequenze idrofobiche che ne riducono drasticamente la solubilità in ambiente acquoso. In condizioni patologiche, la presenza di ioni metallici in concentrazioni non regolate correttamente stimola l'aggregazione dei peptidi Aβ, inducendo la conversione dei motivi ad α-elica in β-foglietti; quest'ultimi si assemblano fino a formare irreversibilmente degli aggregati insolubili, noti come placche o fibrille amiloidi.

Il processo di aggregazione segue una cinetica di nucleazione dipendente dal tempo, articolata in tre fasi principali: (i) fase iniziale detta di "lag" in cui i monomeri del peptide interagiscono formando degli oligomeri; (ii) fase di allungamento in cui i nuclei agiscono come centri di nucleazione per la rapida addizione di ulteriori monomeri, determinando una veloci associazione in protofibrille e aggregati di dimensioni maggiori; (iii) fase stazionaria (a *plateau*) in cui si raggiunge una situazione di equilibrio caratterizzata da fibrille di grosse dimensioni stabili e insolubili (Fig. 5).[4]

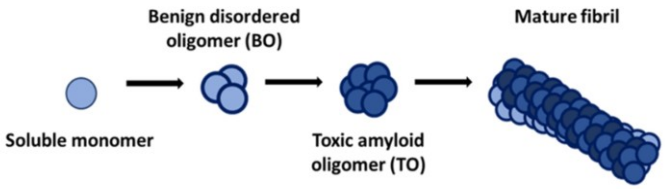

Fig. 5 *Processo di formazione di aggregati amiloidi.*

Lo studio svolto con il complesso texafirinico MnTexCOOH è stato focalizzato sull'inibizione dell'aggregazione del peptide β-amiloide durante la sua fase iniziale. Si suppone che il complesso interagisca con la porzione N-terminale del peptide Aβ quando esso si trova in stato monomerico, impedendo la formazione di oligomeri e di conseguenza di fibrille mature.

Il metallo al centro del complesso lega in posizione assiale l'atomo di azoto del residuo di acido aspartico che si trova all'estremità del peptide, raggiungendo così una esa-coordinazione.

Per valutare l'attività inibitoria della texafirina è stato svolto uno studio preliminare con l'utilizzo di albumina da siero bovino (BSA) come modello, poiché la proteina forma aggregati amiloidi seguendo lo stesso meccanismo di aggregazione dei peptidi Aβ, pur essendo una proteina con dimensioni maggiori rispetto al peptide. Il monitoraggio dell'aggregazione è stato eseguito impiegando il fluoroforo Yat ProteoStat, una molecola la cui emissione di fluorescenza aumenta selettivamente in seguito al legame con aggregati proteici e peptidici. L'esperimento è stato realizzato mantenendo costanti le concentrazioni di BSA e di colorante Yat ProteoStat e aggiungendo concentrazioni crescenti di MnTexCOOH. I campioni sono stati incubati a 65° C per stimolare l'aggregazione della proteina; la misurazione dell'intensità di fluorescenza ha consentito di calcolare la percentuale di inibizione dell'aggregazione indotta dal complesso texafirinico, che ha raggiunto un valore massimo del 76 %.

Lo stesso esperimento è stato svolto con il peptide $A\beta_{40}$, mantenendo fisse le concentrazioni del peptide e della sonda e variando la concentrazione di MnTexCOOH. In seguito a incubazione a 37° C (temperatura fisiologica di aggregazione del peptide), l'analisi di fluorescenza ha mostrato una spiccata attività inibitoria da parte del complesso, raggiungendo una percentuale massima di inibizione pari all'83 %.

Sugli stessi campioni di BSA e peptide $A\beta_{40}$, incubati alla rispettiva temperatura di aggregazione, è stata svolta un'analisi con Dynamic Light Scattering (DLS), con cui è stato possibile osservare la dimensione media degli aggregati formati grazie allo scattering della luce. I profili di scattering hanno evidenziato una netta riduzione del diametro medio delle particelle in presenza di MnTexCOOH rispetto al controllo privo di inibitore, confermando l'efficacia del complesso nel bloccare la crescita degli aggregati. Un'ulteriore analisi è stata effettuata con Atomic Force Microscopy (AFM) sui campioni contenenti il peptide $A\beta_{40}$ con aggiunta di texafirina come inibitore. Dalle immagini ottenute è stato possibile osservare un aggregato peptidico con dimensioni inferiori a 1 μm, un valore notevolmente inferire rispetto alle dimensioni riportate in letteratura relativi ad aggregati peptidici senza la presenza di un inibitore pari a circa 4 μm, confermando l'efficienza dell'inibizione. A partire dai valori di attività inibitoria ottenuti con i saggi con la proteina BSA e il peptide $A\beta_{40}$, è stato possibile determinare il valore IC_{50}, definito come la concentrazione di inibitore necessaria per dimezzare l'aggregazione amiloide *in vitro*.

Infine, come ultimo step dello studio, è stata valutata l'efficacia di MnTexCOOH nell'inibire l'aggregazione del peptide $A\beta_{40}$ espresso *in vivo* all'interno di cellule di *Escherichia coli.* Sono stati

svolti due esperimenti utilizzando un batch di batteri *E. coli*; un primo esperimento è stato realizzato con l'aggiunta diisopropil-β-D-1-tiogalattopiranoside (IPTG) per indurre l'espressione del peptide $A\beta_{40}$ all'interno del batterio, mentre nel secondo esperimento, invece, non è stato aggiunto IPTG per evitare l'espressione del peptide. Ad entrambi i set di campioni è stata aggiunta MnTexCOOH in concentrazioni crescenti ed il colorante Yat Proteostat; dopo incubazione a 37° C, le misure di assorbanza (per la stima della densità cellulare) e di fluorescenza hanno permesso di quantificare l'attività inibitoria, la quale ha raggiunto un valore picco del 77 %. Tali risultati indicano che il complesso texafirinico è in grado di permeare la doppia membrana cellulare tipica dei batteri Gram-negativi come *E.coli*.

Si può concludere affermando che il complesso corrolico FeTCPC mostra un'attività antiossidante di tipo pseudo-perossidasico modesta rispetto a quella del complesso emina; al contrario, il complesso MnTPCMe ha mostrato una notevole attività pseudo-catalasica. Infine, il secondo complesso porfirinoide esaminato, MnTexCOOH, ha rivelato un'elevata efficacia nell'inibire l'aggregazione amiloide, dimostrandosi un valido composto applicabile come possibile terapia nell'ambito delle malattie neurodegenerative.

Al termine dello studio si può affermare che entrambe le categorie di complessi porfirinoidi studiati rappresentano un valido punto di partenza per eventuali studi futuri volti a contrastare lo stress ossidativo e la neurotossicità associata all'aggregazione amiloide.

1. Introduction

1.1 Neurodegenerative diseases

Neurodegenerative pathologies are associated with cognitive decline, and behavioral and physical disability, ultimately leading to death. The two most common diseases are Alzheimer's disease (AD) and Parkinson's disease (PD), although they are two different pathologies, with different symptoms, in both cases protein misfolding and accumulation of amyloid aggregates are observed in the brain, all factors that lead to neuronal death and consequently to the onset of the typical symptoms of these diseases.[2] Given the multifactorial nature of the causes underlying the onset of these diseases and the various mechanisms involved, finding an effective therapy remains extremely challenging. Over the last decade, research has focused on several primary hypotheses regarding the disease's etiology, chief among them being the amyloid cascade hypothesis. In specific brain regions such as the hippocampus, responsible for short-term memory and space-temporal orientation, the presence of senile plaques has been observed. These are protein aggregates composed of approximately 40 amino acids, known as Aβ amyloid plaques, which derive from the transmembrane precursor protein APP.[5]

APP is a protein consisting of about 700 aminoacidic residues; it is cleaved into various fragments by two endoprotease enzymes: α-secretase and β-secretase, which yield, respectively, to a non-amyloidogenic and amyloidogenic pathway (Fig. 1). Following the amyloidogenic pathway, β-secretase is responsible for the first cleavage that generates sAPP-β and C99 fragments, followed by γ-secretase that leads to the production of Aβ monomers. These monomers tend to undergo misfolding, forming oligomers and, subsequently, amyloid fibrils.[6]

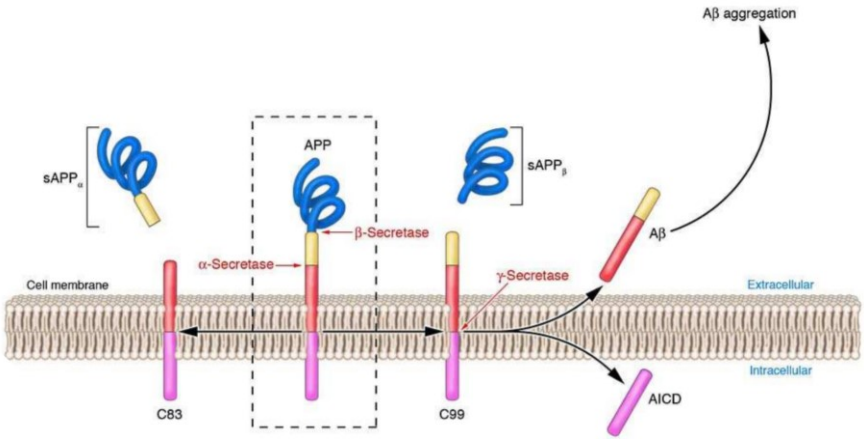

Fig. 1 *Non-amyloidogenic (left) and amyloidogenic (right) pathways of APP cleavage leading to the formation of Aβ peptide.*[6]

Amyloid fibrils are formed through a polymerization process that is nucleation-dependent; the initial α-helical portions of the monomeric Aβ peptide lose their native conformation, converting in β-sheets structures arranged perpendicular to the axis of the fiber, forming a cross-β pattern, a main feature of the amyloid structure. Such structures are stabilized by numerous hydrogen bonds that make them resistant to degradation and inclined to form bigger aggregates.

The process of fibrils formation is a nucleation-dependent polymerization (Fig. 2); the first step is a lag or nucleation phase, followed by an elongation or transition phase during which toxic oligomers are formed, ending with a saturation phase, where mature and highly stable fibrils are produced. The slower step is the formation of polymerized proteins that work as seeds, facilitating the following formation of amyloid fibrils.[4]

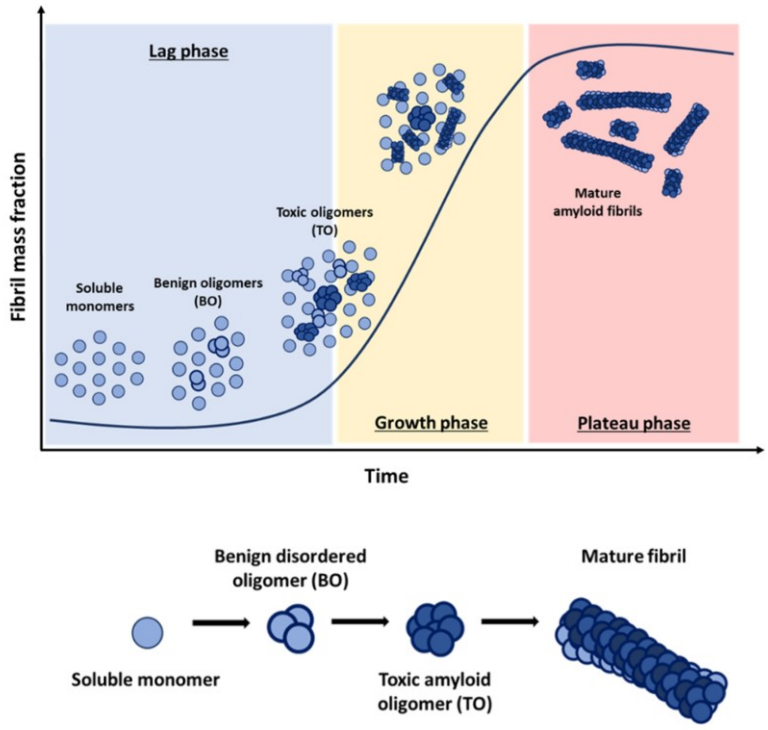

Fig. 2 *Schematic representation of Aβ peptides aggregation process.* [7]

The formation of these plaques is further amplified by the presence of dysregulated concentrations of redox-active metals in certain areas of the brain; this phenomenon introduces an additional hypothesis among the causes of the disease's onset.

1.2 Role and activity of metals

Transition metal ions, particularly Fe, Cu, and Zn, play a key role in the development of neurodegenerative diseases, due to their interaction with Aβ peptides and their catalysis of reactive oxygen species (ROS) production, which leads to oxidative stress condition.

The interaction between these metals and Aβ peptides occurs through the coordination of the metal center to specific residues, in particular histidine (H6, H13, H14), located along the peptide chain, as highlighted in the $A\beta_{1\text{-}40}$ aminoacidic sequence described below. This coordinative bonding induces a misfolding of the chain, which folds upon itself to form insoluble amyloid plaques.[8]

DAEFR**H**DSGYEV**HH**QKLVFFAEDVGSNKGAIIGLMVGGVV

In particular, the Cu^{2+} ion binds the amino acids through a penta-coordination involving oxygen and nitrogen atoms, four of which are located in the equatorial plane and one in the axial position (Fig. 3).[8]

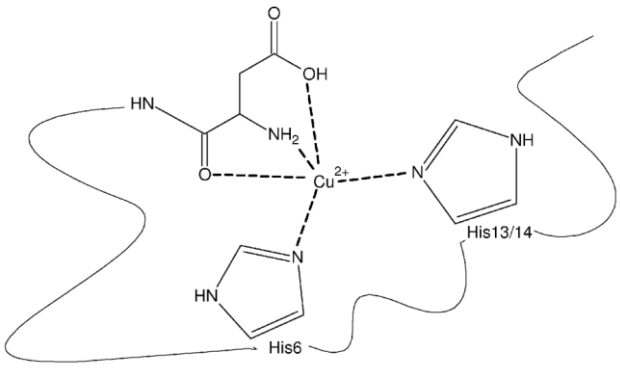

Fig. 3 *Cu^{2+}-Aβ coordination scheme.*

Iron, on the other hand, can be found free or bound to protoporphyrin IX. This complex is called heme when the iron is in the 2+ oxidation state, or hemin when the iron is in the 3+ oxidation state. Free hemin can form hexa-coordinated complex with Aβ peptide by binding two histidine residues in the axial positions (Fig. 4).

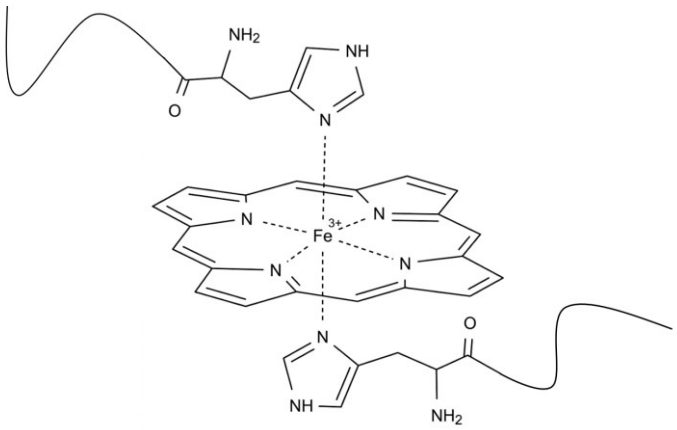

Fig. 4 *Hemin- Aβ coordination scheme.*

Moreover, redox-active transition metal ions such as iron and copper play a key role in ROS production, whether in their free or bound to macrocycles. The main ROS are superoxide ($O_2^{\bullet -}$), dihydrogen peroxide (H_2O_2), and hydroxyl radical ($OH^{\bullet}$); these species are formed under all oxidative conditions in the mitochondria as a side product of oxidative metabolism.
The enzymes involved in the body's antioxidant system catalyze ROS disproportionation, converting them into harmless species; examples include catalase (CAT) and superoxide dismutase (SOD).

Under normal physiological conditions, approximately 1% to 3% of molecular oxygen is converted into ROS. In this context, these species are not harmful, as their activity is countered by an endogenous antioxidant defense system.[2] However, in pathological conditions, ROS production significantly increases, and the antioxidant system is unable to neutralize them. This excess of ROS leads to a state known as oxidative stress, resulting in oxidative damage to various cellular components such as proteins, lipids, and DNA ultimately leading to neuronal cell death.

The overproduction of ROS is catalyzed by transition metals through Fenton and Haber-Weiss reactions; Fenton reaction shows the oxidation process of Fe(II) involving hydrogen peroxide that leads to the splitting of the peroxide forming hydroxyl radical and hydroxide ion. Haber-Weiss describes the reaction of peroxide with superoxide radical forming oxygen, hydroxyl radical and hydroxide anion, catalyzed by a metal ion. The combination of these two reaction processes results in what is known as the Haber-Weiss cycle (Fig. 5).

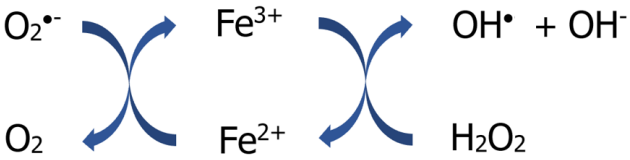

Fig. 5 *Fenton/Haber-Weiss cycle.*

The metal in its reduced form reacts with hydrogen peroxide (H_2O_2) leading to the formation of hydroxide radical ($OH^{\bullet}$), a strongly oxidizing species, while the metal oxidizes. The interaction with superoxide radical ($O_2^{\bullet-}$) brings back the metal to the reduced state so the process can start from the beginning.[2]

1.3 Porphyrinoid macrocycles - Corroles

A possible therapy against neurodegenerative diseases is based on inhibiting the aggregation of Aβ peptides into amyloid plaques and limiting the oxidative and harmful activity of ROS converting them into inactive species. With this purpose, metal complexes containing porphyrinoid macrocycles with an antioxidant activity are introduced and corroles represent a primary class of these compounds.

Corroles are tetrapyrrolic macrocycles with one carbon atom less than porphyrin and one additional NH proton in their inner core (Fig. 6). Corroles are tri-anionic ligands that, thanks to their contracted cavity, stabilize metal ions in unusually high oxidation states of the metal ion they host, such as Fe(IV) and Mn(III). Despite having one less carbon atom, these macrocycles maintain the same aromaticity as porphyrins since they always possess 18 π-electrons.[9]

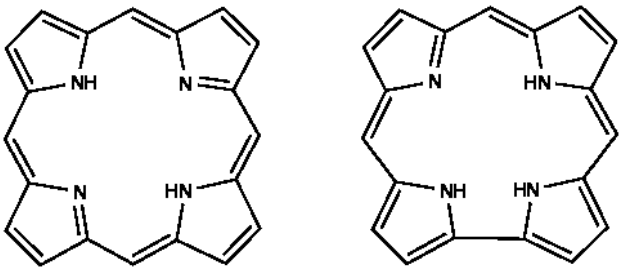

Fig. 6 *Porphyrin and corrole structures.*

This type of system is well-known in the literature for various applications, the foremost of which is photodynamic therapy (PDT).[10] This therapy relies on the combination of a photosensitizer, in this case a porphyrinoid compound, with molecular oxygen to target and destroy cancer cells. Upon irradiation, the macrocycle reaches an excited singlet state and subsequently, through an Intersystem Crossing process, a triplet state. This triplet state possesses a sufficiently long lifetime to interact with stable triplet oxygen and generate a highly reactive singlet oxygen. Singlet oxygen is a powerful oxidant that reacts with a variety of biological molecules; therefore, the site of the production of this specie determines which cells are going to be attacked and damaged.

A second application of corroles is the stabilization of DNA G-quadruplex structures.[11] These are folds in the guanine-rich terminal portions of chromosomes; such structures protect the ends of chromosomes, shielding them from harmful processes during replication phases. The enzyme telomerase, which is responsible for telomere cleavage, is overexpressed in cancer cells; however, if the telomere is folded into a G-quadruplex structure, telomerase activity is inhibited, leading to the destruction of tumor cells while sparing healthy ones.

Positively charged corrole complexes, containing metals in high oxidation states such as Cu(II) and Mn(III), interact with high affinity with G-quadruplexes, thereby stabilizing their structure. Therefore, this type of complexes represents a key strategy in the design of antitumor agents.

Another particularly relevant application of corrole complexes is their use as antioxidant agents capable of counteracting oxidative and nitrative stress caused by an excess of ROS and Reactive nitrogen species (RNS).

Corrole complexes containing redox-active metals such as iron and manganese have been developed to function as biomimetics of the natural enzymes catalase and superoxide dismutase (SOD). Superoxide dismutase converts the superoxide radical into biologically harmless species, while catalase functions by decomposing hydrogen peroxide molecules into water and molecular oxygen.[12]

SOD catalyzed reaction: $2\,O_2^{\cdot -} + 2H^+ \rightarrow O_2 + H_2O_2$

Catalase catalyzed reaction: $2\,H_2O_2 \rightarrow O_2 + 2\,H_2O$

As previously mentioned, corroles also act by countering the nitrative stress caused by an excess of RNS. These complexes can be applied as scavengers for such species, particularly the peroxynitrite anion ($ONOO^-$), which is a highly aggressive and oxidizing agent.[13]

1.4 Porphyrinoid macrocycles - Texaphyrins

Another category of porphyrinoids, the texaphyrins, is also being studied for the same ROS and RNS scavenger application. Texaphyrins are Schiff base macrocyclic complexes containing one additional nitrogen atom compared to the porphyrin ring (Fig. 7); texaphyrins contain approximately 20% larger core and display a unique electronic structure.

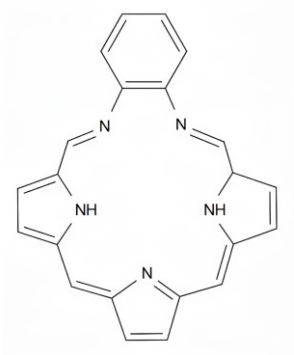

Fig. 7 *Texaphyrin structure.*

In particular, Mn(II) texaphyrin have shown efficient antioxidant and antinitrative activity through catalytic mechanisms close to those of Mn(III) corroles. The ligand expanded macrocycle stabilizes the manganese ion across multiple oxidation states enabling rapid electron transfer rates. A primary feature of these complexes is their capacity to scavenge peroxynitrite, a highly reactive species responsible for nitrative stress, via decomposition into non-toxic compounds: nitrate (NO_3^-) and nitrite (NO_2^-) anions. Furthermore, Mn(II) texaphyrins function as effective mimics of both superoxide dismutase (SOD) and catalase enzymes.

Texaphyrin complexes can also be widely utilized as MRI contrast agents: systems containing paramagnetic metals such as Gd(III) and Mn(II) are employed as contrast agents for detecting Aβ amyloid plaques. Indeed, the paramagnetic properties of the metal make texaphyrins particularly suitable for detecting Aβ aggregates at high magnetic fields.[3] The complex's paramagnetic metal, in the presence of Aβ aggregates, causes an increase in the relaxation times of the surrounding water protons (the R1 parameter, which relates to longitudinal proton relaxation) compared to the times measured with a control protein, such as albumin. This effect is more pronounced in the presence of Aβ aggregates than in the presence of the peptide in its monomeric form. The increase in R1 results in a stronger MRI signal in the regions where amyloid Aβ aggregates are located, facilitating their localization, which can be used for facilitating the diagnosis process and treatments of neurodegenerative diseases.

The complex binds to Aβ oligomers and fibrils through an axial bond between the metal and the amino acids of the peptide and, in particular, Mn(II) shows high affinity towards histidine residues (H6, H13, H14) which coordinates to form a complex with octahedral geometry.

Furthermore, hydrophobic interactions with apolar zones of the aggregate are also involved and π-π stacking interactions with aromatic residues of aminoacids like phenylalanine (F19, F20) and tyrosine (Y10); as a result, the complex becomes embedded within the aggregate structure.

DAEFR**H**DSG**Y**EV**HH**QKLV**FF**AEDVGSNKGAIIGLMVGGVV

Once bound, the texaphyrin is capable of altering the structural composition of the Aβ fibrils, reducing the percentage of β-sheets and transforming the fibrils into amorphous structures. This suggests that it could influence the aggregation of Aβ peptides, consequently reducing their toxicity.[3]

2. Aim of the thesis

The primary objective of this study was to identify compounds capable of exhibiting antioxidant activity against ROS through peroxidase-like and catalase-like functions.

In order to study the antioxidant activity of these compounds, two corrolic complexes were synthesized and characterized (Fig. 8) following synthesis procedure described in the literature: Fe(IV)-5,10,15-tris(p-carboxyphenyl) corrole (FeTCPC) and Mn(III)-5,10,15-tris(N-methyl-4-pyridyl) corrole (MnTPCMe).

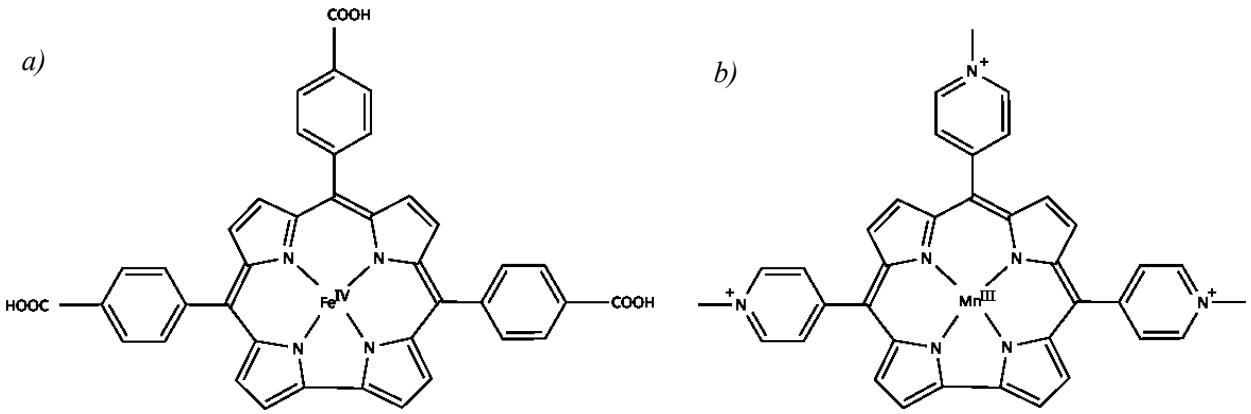

Fig. 8 *FeTCPC (a) and MnTPCMe (b) complexes structures.*

As an initial analysis of the study, the pseudo-peroxidase activity (at the expense of a substrate that is oxidized) of the FeTCPC complex was evaluated, using hemin as a reference system. Two substrates were used: 3-(4-hydroxyphenyl)propionic acid (HPA) and 4-methylcatechol, by monitoring the absorption band of their respective oxidation products, it was possible to determine the rate of the oxidation reaction. Subsequently, the parameters indicating the rate at which the substrate is converted into the product and the apparent affinity between the catalyst and the substrate were determined.

The next phase of the study was focused on th the catalase-like activity of the MnTPCMe complex which was tested through a kinetic analysis and compared with bovine liver catalase, used as a reference enzyme, whose catalyzed reaction involves the dismutation of hydrogen peroxide.

The second phase of the study was conducted at Professor Gamez's Chemistry department and Professor Sabatè's Pharmacy department at the University of Barcelona, in collaboration with University of Pavia. This section was focused on the ability to inhibit the aggregation of β-amyloid (Aβ) peptides into insoluble plaques.

The study conducted with the texaphyrin complex manganese(II)-(9,24-hydroxypropyl-17-carboxyl)-texaphyrin (MnTexCOOH) (Fig. 9) focused on inhibiting the aggregation of the β-amyloid peptide during its initial phase.

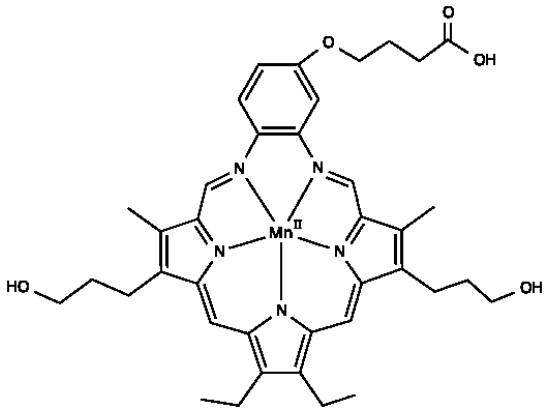

Fig. 9 *MnTexCOOH complex structure.*

A preliminary study was conducted using bovine serum albumin (BSA) as a model, since this protein forms amyloid aggregates via the same aggregation mechanism as Aβ peptides, despite having a different size. At first, aggregation was monitored using the Yat ProteoStat fluorophore, a dye that emits fluorescence when bound to protein and peptide aggregates, based on the data obtained, the inhibitor concentration required to reduce aggregation by 50% was calculated (IC_{50}) for both BSA and $A\beta_{40}$ peptide. Thereafter, DLS and AFM techniques were used in order to observe the reduction of the aggregates dimension, compared with those of aggregates formed in the absence of the inhibitor.

Finally, as the last section of the study, the efficacy of MnTexCOOH in inhibiting the aggregation of the $A\beta_{40}$ peptide expressed in vitro within *Escherichia coli* cells was evaluated in order to test not only its inhibitory activity but also the permeability of the texaphyrin complex through the bacterium's double lipid membrane.

3. Results and discussion

3.1. Synthesis and Characterization of porphyrinoid complexes

3.1.1. Synthesis and Characterization of FeTCPC

Synthesis of FeTCPC complex (Fig. 10) is reported in paragraph 4.2. in "Materials and methods" chapter; the process started with the production of the ligand H_2TCPC and its purification via HPLC, the second step is the metallation of the ligand using $FeCl_2$ and purification of the complex through coloumn chromatography. The last step was the deprotection of the carboxyl functional groups that occurs through a basic hydrolysis reaction using an excess of KOH, followed by an acidic wash using HCl and the last purification through HPLC.

a)

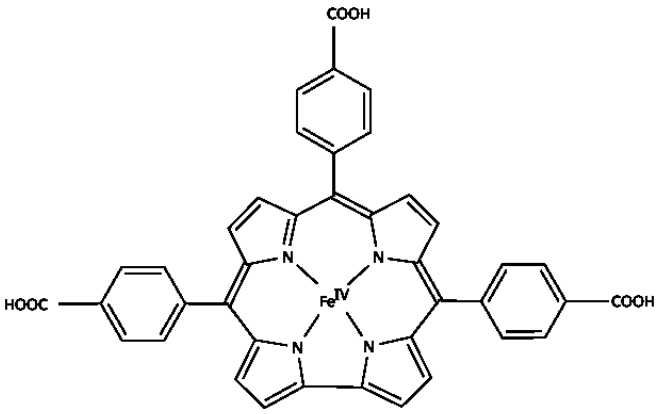

b)

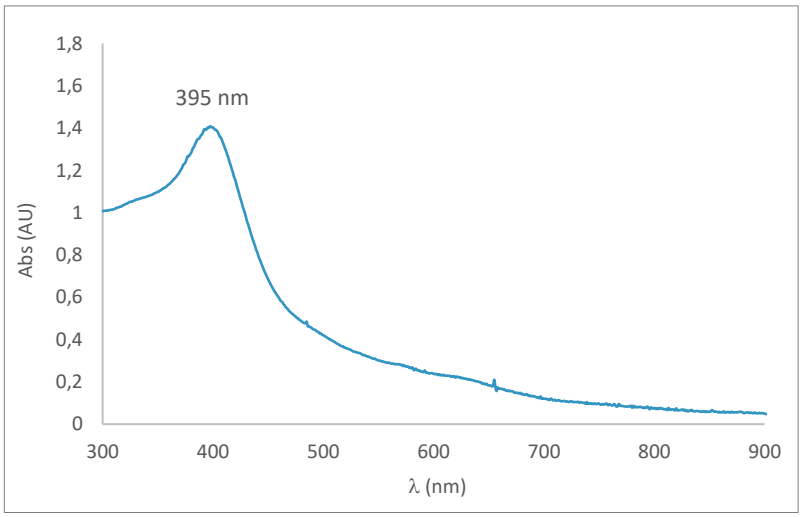

Fig. 10 *a) FeTCPC structure and b) UV-Vis spectra performed in MeOH (ε = 35000 M^{-1} cm^{-1}).*[14]

3.1.2. Synthesis and Characterization of MnTPCMe

Synthesis of MnTPCMe complex (Fig. 11) is reported in paragraph 4.3. in "Materials and methods" chapter; the process started with the production of the ligand H_2TPC and its purification via coloumn chromatography, with two consecutive coloumn purifications. The second step is the metallation of the ligand using $(CH_3COO)_2Mn \cdot 4H_2O$ salt and purification of the complex through coloumn chromatography. The last step consists of the methylation of the pyridil functional groups, carried outwith the addition of methyl iodide to the purified complex.

a)

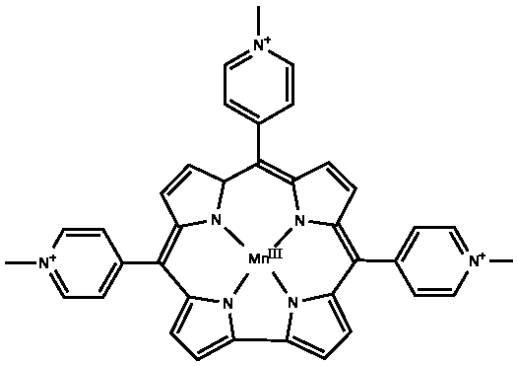

b)

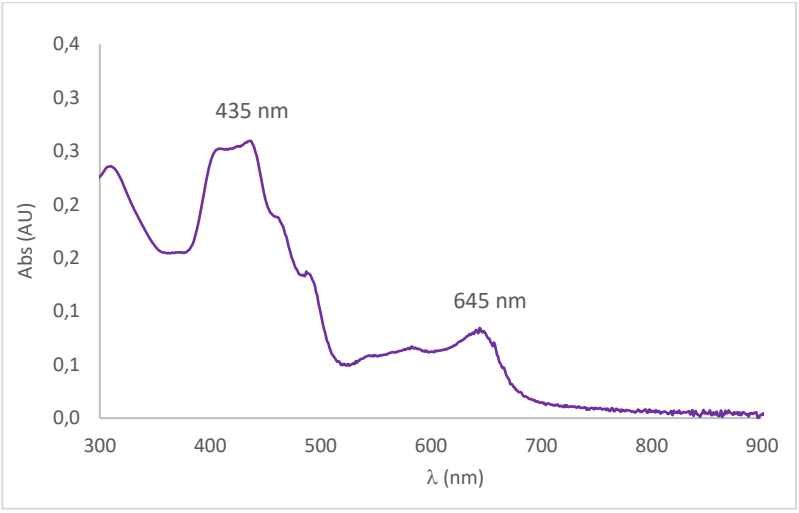

Fig. 11 *a) MnTPCMe structure and b) UV-Vis spectra performed in MeOH (ε = 36000 M^{-1} cm^{-1}).*[15]

3.1.3. Characterization of MnTEXCOOH

a)

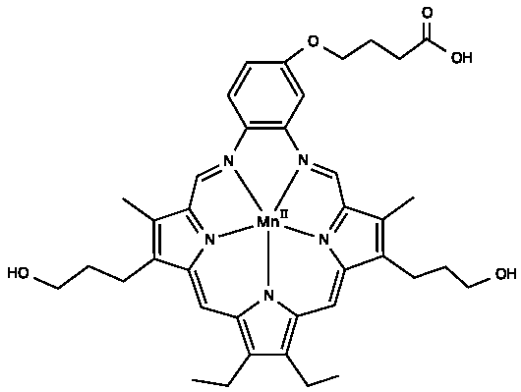

b)

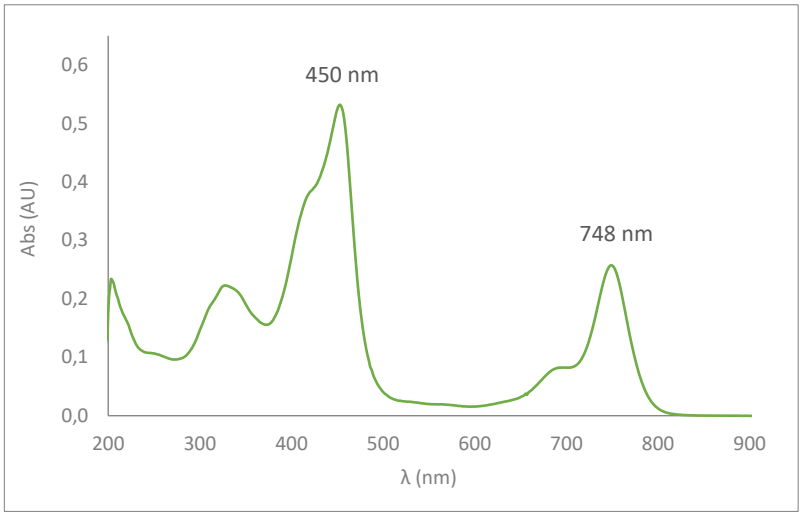

Fig. 12 *a) MnTexCOOH structure and b) UV-Vis spectra performed in MeOH (ε = 60900 M^{-1} cm^{-1}).*

For MnTexCOOH complex (Fig. 12) two molar extinction coefficients (ε) have been determined experimentally, one in native buffer (NB) (50 mM Tris·HCl, 150 mM NaCl at pH 7,4) and one in MeOH. The determination has been performed with a spectrophotometric titration in both cases using a MnTexCOOH solution whose concentration has been determined through weighing the solid compound. To calculate the result of the ε in MeOH, other experimental tests conducted in the laboratory were also involved. The results of ε in different solvents are presented below:

$$\varepsilon \text{ (NB)} = 30760 \text{ M}^{-1} \text{ cm}^{-1}$$

$$\varepsilon \text{ (MeOH)} = 60900 \text{ M}^{-1} \text{ cm}^{-1}$$

3.2. Reactivity studies

3.2.1. Peroxidase-like activity of FeTCPC

Peroxidases are a family of heme enzymes whose function is to catalyze the reduction of hydrogen peroxide (H_2O_2) through the donation of electrons by a reducing substrate. In pathological contexts, such as neurodegenerative diseases, it is essential to reduce hydrogen peroxide in order to render it harmless and block the production of reactive oxygen species (ROS) that can cause oxidative stress within the brain.

In this study the focus will be on the activity that mimics the function of plant peroxidases, such as (HRP), which are used as reference enzymes. This class of enzymes contain iron-heme b (Fe-protoporphyrin IX functionalized with two methyl, two vinyl and two propionyl substituents) at the active site and carry out the reduction of hydrogen peroxide through a cycle involving three reactions, as shown in Fig. 13.

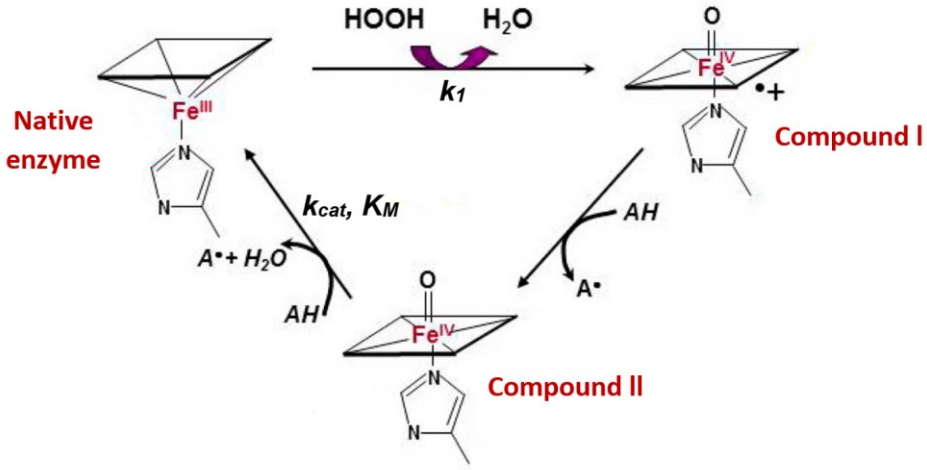

Fig. 13 *Peroxidase catalytic cycle*.[16]

$$[Fe(III) - Por] + H_2O_2 \rightarrow [Fe^{IV} = O - Por^{\bullet+}] + H_2O \qquad (1)$$

$$[Fe^{IV} = O - Por^{\bullet+}] + AH \rightarrow [Fe^{IV} = O - Por] + A^{\bullet} + H^{+} \qquad (2)$$

$$[Fe^{IV} = O - Por] + AH \rightarrow [Fe(III) - Por] + A^{\bullet} + H_2O \qquad (3)$$

The catalytic cycle begins with reaction (1), in which the Fe(III) of the enzyme's heme center in its resting form reacts with the peroxide molecule that binds to the metal center. Distal histidine and arginine play a fundamental role in both the binding and orientation of the peroxide in the distal

pocket. Thanks to the presence of these two amino acids, the central bond between the two oxygen atoms is polarized, causing a heterolytic cleavage of the bond. The distal histidine acts both as a proton acceptor from the first of the two oxygen atoms in the peroxide and as a proton donor to the second. In this way, one oxygen atom leaves the enzyme pocket in the form of a water molecule, while the second remains bound to the metal center. An electron is donated by iron to form the ferryl intermediate, while a second electron is donated by the porphyrin ring, which is converted into a radical-cation species, forming Compound I.

In the second step of the process (2), Compound I is converted into the intermediate species defined as Compound II, a compound that again contains the ferryl species. Through an oxidation reaction of a substrate (AH), the porphyrin ring stabilizes by gaining an electron, while the substrate is converted into the corresponding radical species (A•). The process of returning to the enzyme's native form and completing the catalytic cycle requires a further reaction (3) involving the oxidation of a substrate (AH) with the production of a water molecule. The third and final stage of the catalytic cycle is the slowest, and therefore represents the rate-determining step.[16]

As can be seen from the diagram of the catalytic cycle (Fig. 12), the rate of the first step in the cycle depends on the kinetic constant k_1 and the concentration of H_2O_2; it is described by the following equation: [17]

$$v = k_1 \cdot [cat] \cdot [H_2O_2]$$

The reaction rate increases proportionally with peroxide concentration, following a hyperbolic trend, until it reaches a saturation concentration, after which the reaction rate begins to decrease.

The saturating concentration of peroxide is subsequently held constant and used for the kinetic study of the third stage of the catalytic cycle, in which the concentration of the substrate to be oxidized by the heme center is increased; the kinetics of this step are approximated by the Michaelis-Menten model. The constant k_{cat} represents the enzyme's turnover number; it thus indicates the number of substrate molecules that the enzyme converts per unit time under saturating substrate conditions. The K_M constant, on the other hand, is the Michaelis-Menten constant and represents the substrate concentration (AH) at which the reaction rate is equal to half the maximum rate. The value of K_M expresses the affinity between the enzyme and the substrate.[18]

$$v = \frac{k_{cat} \cdot [cat] \cdot [AH]}{K_M + [AH]}$$

Species with a porphyrin structure similar to the heme one also show an activity defined as pseudo-peroxidase activity, breaking down hydrogen peroxide by following the same reaction steps as peroxidases. In this study, the FeTCPC complex is examined, and its pseudo-peroxidase activity is compared to the one of hemin, using two different substrates: 3-(4-hydroxyphenyl)propionic acid (HPA) and 4-methylcatechol. We are aware that considering the same mechanism for the two compounds is an approximation, since for ferro-corrole there are no studies available that have allowed the characterization of the reaction intermediates for the pseudo-peroxidase reaction.

3.2.1.1. HPA

The first substrate used in this study is HPA (Fig. 14). When oxidized, this compound forms a dimer that exhibits an absorption band at approximately 300 nm, which makes it possible to observe that oxidation has occurred.[1]

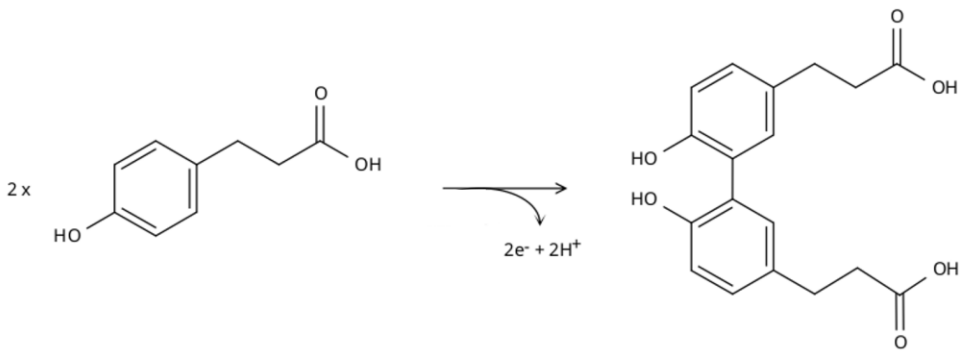

Fig. 14 *HPA oxidation reaction scheme.*

Dependence on hydrogen peroxide concentration

In this step of the kinetic study, the objective is to calculate the value of k_1 constant and determine the saturating concentration of peroxide. The experiment was conducted using FeTCPC and hemin as catalysts for comparison. We then proceeded by conducting an experiment in which the substrate concentration (3 mM) and catalyst concentration (2 μM) were kept constant, while the H_2O_2 concentration was varied (1–75 mM). The experimental procedure is described in paragraph 4.5.1.1. in "Materials and methods" chapter.

The graph below (Fig. 15) shows a comparison of the pseudo-peroxidase activity of FeTCPC and hemin; from the data points, it is possible to identify the saturating concentration of peroxide. To calculate the constant, the first data points from the kinetic study (Fig. 16) are considered, where the concentration of added H_2O_2 is low.

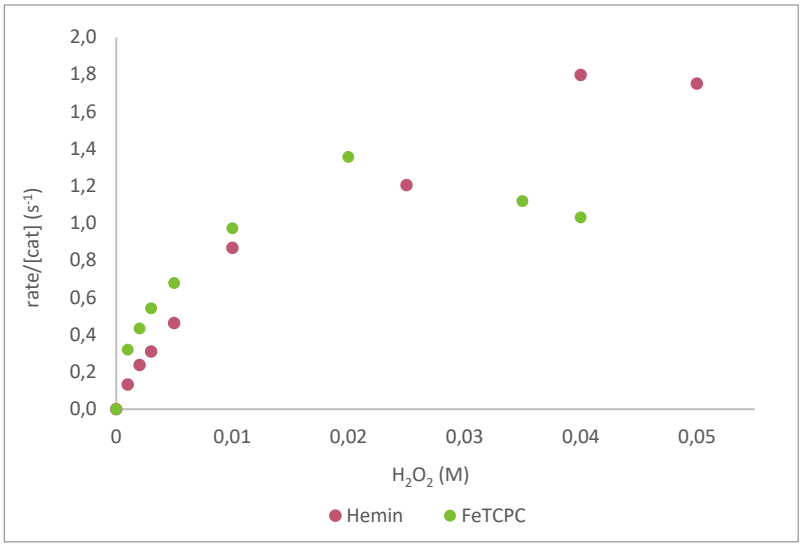

Fig. 15 *HPA oxidation reaction rate with constant concentration of HPA (3 mM), hemin (2 µM), FeTCPC (2 µM) and increasing concentration of H_2O_2 (0 – 75 mM) in phosphate buffer 20 mM pH 7,4.*

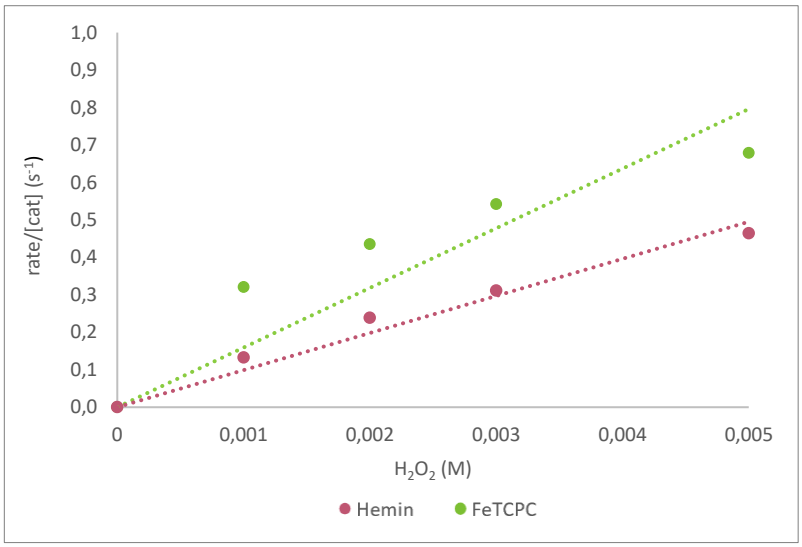

Fig. 16 *Reaction rate data used for the determination of k_1 constant; constant concentration of HPA (3 mM), hemin (2 µM), FeTCPC (2 µM) and increasing concentration of H_2O_2 (0 – 75 mM) in phosphate buffer 20 mM pH 7,4.*

The results of the calculation of k_1 constant for hemin and FeTCPC catalysts, along with their respective determined saturating peroxide concentrations, are shown in the table below:

	k_1 ($M^{-1}s^{-1}$)	$[H_2O_2]_{sat.}$ (mM)
Hemin	83,86 ± 0,04	40
FeTCPC	85,7 ± 0,2	20

Tab. 1 *k_1 constant values for Hemin and FeTCPC with saturating concentrations of H_2O_2.*

From the results obtained for the constants, it's possible to observe that the values for hemin and FeTCPC are very similar; the two compounds have the same ability to activate peroxide in the first step of the peroxidase cycle. The saturating concentrations of H_2O_2 derived from the peaks in the oxidation curves of the experiments conducted can also be noticed.

Dependence on substrate concentration

In the second step of the kinetic study, the goal is to calculate the values of k_{cat} and K_M constants in the Michaelis-Menten equation based on the rate at which the substrate oxidation reaction occurs. Here, a fixed saturating concentration of H_2O_2 (40 and 20 mM) is used, along with that of the catalyst (2 µM), while varying the substrate concentration (0,3–3,5 mM).

The graphic below (Fig. 17) shows a comparison between the pseudo-peroxidase activity of FeTCPC and that of hemin; from the data points, it is possible to determine k_{cat} and K_M values.

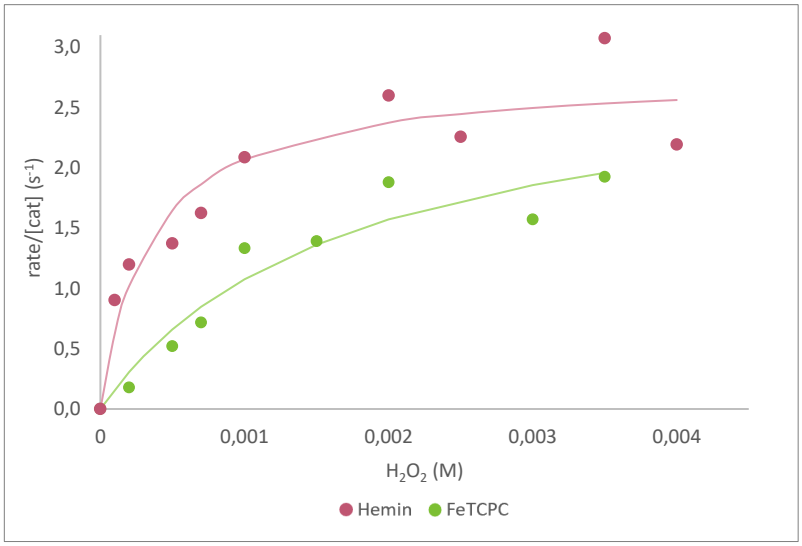

Fig. 17 *HPA oxidation reaction rate with constant concentration of H_2O_2 (40 mM for Hemin and 20 mM for FeTCPC) Hemin (2 µM), FeTCPC (2 µM) and increasing concentration of HPA (0,3 – 3,5 mM) in phosphate buffer 20 mM pH 7,4.*

	K_M (M)	k_{cat} (s^{-1})
Hemin	$3{,}46 \cdot 10^{-4} \pm 1{,}24 \cdot 10^{-4}$	$2{,}78 \pm 0{,}24$
FeTCPC	$1{,}71 \cdot 10^{-3} \pm 5{,}73 \cdot 10^{-4}$	$2{,}91 \pm 0{,}46$

Tab. 2 *K_M and k_{cat} constant values for Hemin and FeTCPC.*

The results show that the K_M value for the FeTCPC complex is higher than that calculated for hemin, indicating that FeTCPC has a lower affinity for the substrate than hemin. The k_{cat} value, on the other hand, is higher for the corrole complex, indicating that its turnover rate and oxidizing power are slightly higher than those of hemin.

3.2.1.2. 4-methylcathecol

4-methylcatechol (4-MC) is used as a second substrate in the study of peroxidase activity; when oxidized, it leads to the formation of 4-methylquinone and subsequently to dimeric products. The dimeric species exhibit an absorption band at approximately 490 nm, and absorption at this wavelength is observed during the kinetic study.

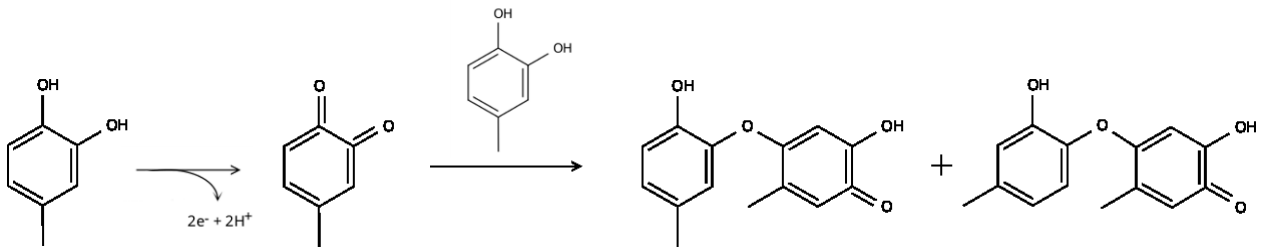

Fig. 18 *4-MC oxidation reaction scheme.*

Dependence on hydrogen peroxide concentration

In this step, we calculate the value of the constant k_1 and determine the saturating concentration of peroxide, using hemin and FeTCPC as catalysts; we then conduct an experiment by keeping the concentrations of the substrate (1 mM) and the catalyst (0,2 μM) constant, while increasing the concentration of H_2O_2 (1 – 400 mM). The experimental procedure is described in paragraph 4.5.1.2. in "Materials and methods" chapter. The graphic below (Fig. 19) shows a comparison of the pseudo-peroxidase activity of FeTCPC and hemin; from the data points, it is possible to determine the saturating concentration of hydrogen peroxide. To calculate the constant, the first data points from the kinetic study (Fig. 20) are considered, where the concentration of added H_2O_2 is low.

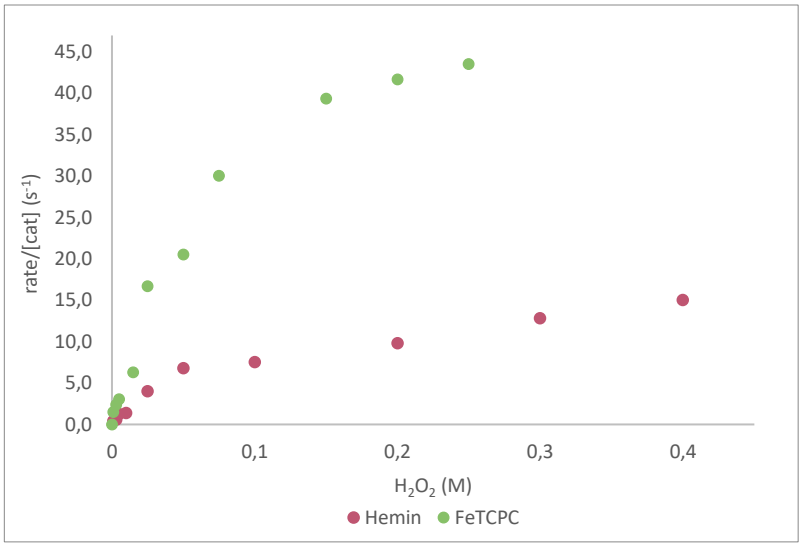

Fig. 19 *4-MC oxidation reaction rate with constant concentration of 4-MC (1 mM), Hemin (0,2 µM), FeTCPC (0,2 µM) and increasing concentration of H_2O_2 (1 – 400 mM) in phosphate buffer 20 mM pH 7,4.*

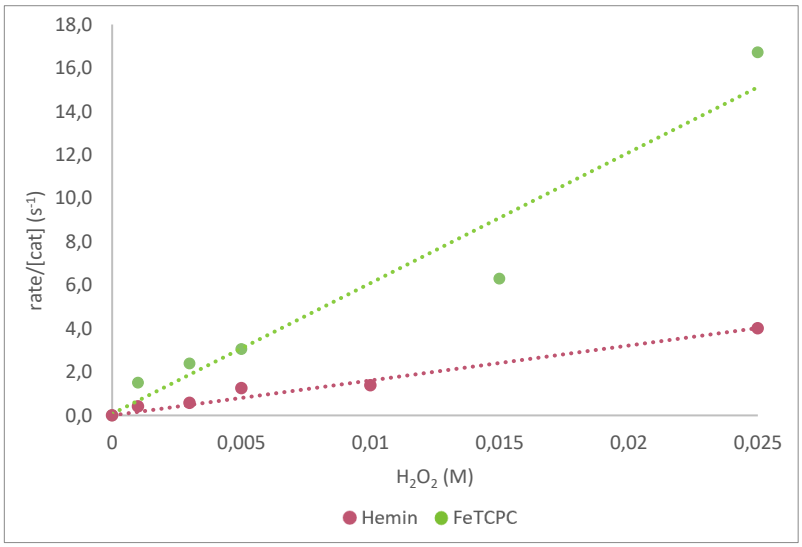

Fig. 20 *Reaction rate data used for the determination of k_1 constant; constant concentration of 4-MC (1 mM), Hemin (0,2 µM), FeTCPC (0,2 µM) and increasing concentration of H_2O_2 (1 – 400 mM) in phosphate buffer 20 mM pH 7,4.*

	k_1 ($M^{-1}s^{-1}$)	$[H_2O_2]_{sat.}$ (mM)
Hemin	152,02 ± 0,15	400
FeTCPC	601,49 ± 0,07	250

Tab. 3 *k_1 constant values for Hemin and FeTCPC with saturating concentrations of H_2O_2.*

The results obtained from the constants show that the FeTCPC complex has a greater ability to activate peroxide in the first step of the peroxidase cycle than hemin. The saturating concentrations of H_2O_2 can also be observed from the peaks in the oxidation curves of the experiments conducted.

Dependence on substrate concentration

In the second step of the kinetic study, the values of k_{cat} and K_M constants are calculated based on the rate at which the substrate oxidation reaction occurs. A fixed saturating concentration of H_2O_2 (400 and 250 mM) is used, along with that of the catalyst (0,2 µM), while the substrate concentration is varied (0,3–3,5 mM).

The graphic below (Fig. 21) shows a comparison between the pseudo-peroxidase activity of FeTCPC and that of hemin; from the data points, it is possible to determine k_{cat} and K_M values.

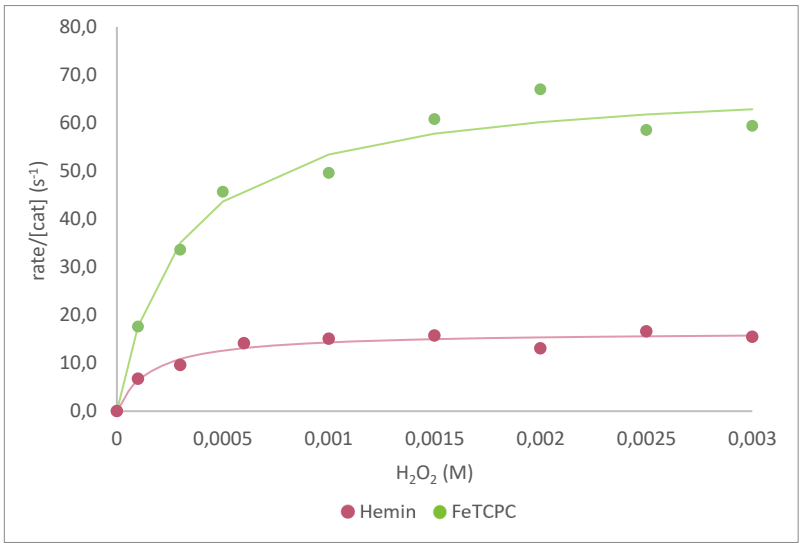

Fig. 21 *4-MC oxidation reaction rate with constant concentration of H_2O_2 (400 mM for hemin and 250 mM for FeTCPC), hemin (0,2 µM), FeTCPC (0,2 µM) and increasing concentration of 4-MC (0,1 – 3 mM) in phosphate buffer 20 mM pH 7,4.*

	K_M (M)	k_{cat} (s^{-1})
Hemin	$1{,}58 \cdot 10^{-4} \pm 4{,}25 \cdot 10^{-5}$	$16{,}57 \pm 0{,}78$
FeTCPC	$2{,}90 \cdot 10^{-4} \pm 5{,}73 \cdot 10^{-5}$	$68{,}94 \pm 3{,}10$

Tab. 4 *K_M and k_{cat} constant values for Hemin and FeTCPC.*

From the calculation of the constants, a higher K_M value is observed for the FeTCPC complex compared to that calculated for the hemin; in fact, FeTCPC exhibits a lower affinity for the substrate than the hemin. The corrole complex, however, exhibits a higher k_{cat} value than that of the hemin, indicating that the oxidizing power and turnover rate for FeTCPC are slightly higher than those of the hemin, consistent with the results obtained for the constants calculated for the HPA substrate.

The significantly higher k_{cat} observed for 4-MC compared to HPA is fundamentally attributed to their distinct chemical structures. The presence of two adjacent electron-donating hydroxyl groups, complemented by the weak inductive electron-donating methyl group on 4-MC, significantly increases the electron density of the aromatic ring. Consequently, catechols display a substantially lower oxidation potential than monophenols because the resulting semiquinone radical intermediate is strongly stabilized by resonance and intramolecular interactions. This facilitates electron transfer to the enzyme's active site, resulting in a much faster turnover rate for 4-MC.

3.2.2. Catalase-like activity of MnTPCMe

The enzyme catalase belongs to the heme-protein family; it consists of four subunits, each containing a heme group. The Fe(III) ion present in each subunit is redox-active and plays a key role in the reaction that breaks down two molecules of hydrogen peroxide into one molecule of water and one of oxygen.

$$[Fe(III) – Por] + H_2O_2 \rightarrow [Fe^{IV} =O – Por^{\bullet+}] + H_2O \qquad (1)$$

$$[Fe^{IV} =O – Por^{\bullet+}] + H_2O_2 \rightarrow [Fe(III) – Por] + O_2 \qquad (2)$$

The catalytic process consists of two single-electron transfer steps: in the first step, the iron in the heme group is oxidized to form a radical cation complex (indicated as $Por^{\bullet+}$ reaction (1) and (2)) and iron(IV)-oxo species, releasing a water molecule; in the second step, the complex oxidizes a second molecule of H_2O_2 via another two-electron reduction, returning the heme to its native Fe(III) state while generating molecular oxygen and a second water molecule. [19]

In this study the focus is on a Mn(III) corrole complex; manganese, unlike iron, is poorly suited for promoting oxidation reactions, like cleavage of hydrogen peroxide. Instead, in biological systems, manganese complexes are well suited for antioxidant activity, as demonstrated by the Mn-containing superoxide dismutase (SOD) enzyme.
The purpose of this experiment is to test the pseudo-catalytic activity of a non-heme complex: MnTPCMe. The experiment was conducted using ABTS (2,2'-azinobis[3-ethylbenzothiazoline-6-sulfonic acid]), a compound that is oxidized by H_2O_2 if the latter is present in the reaction medium in the presence of a catalyst, as shown in Fig. 22.

A decrease in the absorption band at 660 nm of the ABTS radical cation oxidation product is observed; from the intensity of this band, it is possible to deduce how much peroxide was disproportionated by the catalyst under investigation.

In this study, the activity of the MnTPCMe complex was analyzed using bovine liver catalase as the reference enzyme, in both cases in the presence of horseradish peroxidase (HRP) as the catalyst for the oxidation reaction.

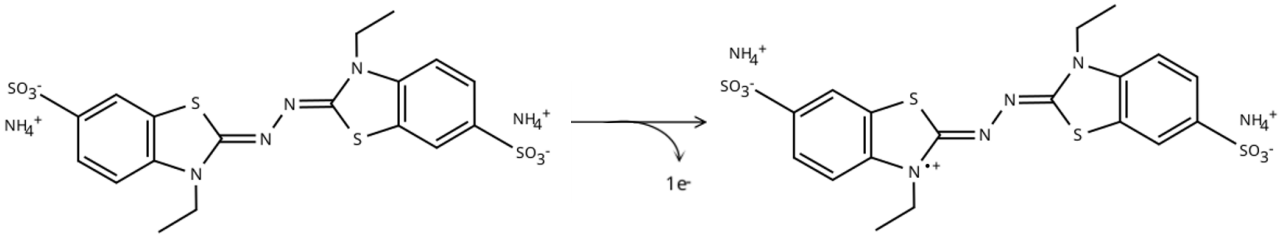

Fig. 22 *Oxidation reaction of ABTS in presence of H_2O_2 and a catalyst.*

The graphic below shows the curves for peroxide without pseudo-catalase enzymes, with the addition of bovine catalase, and with the addition of MnTPCMe (Fig. 23).

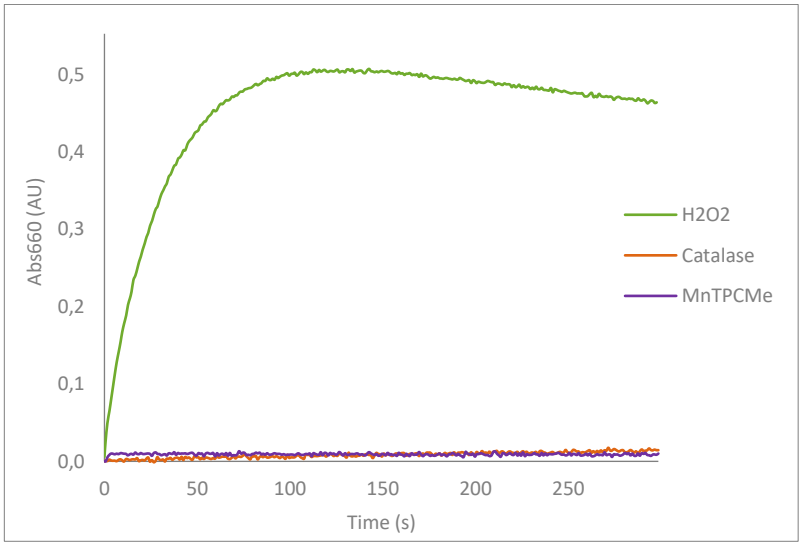

Fig. 23 *ABTS oxidation profile without enzyme and in presence of bovine catalase and MnTPCMe.*

The curves shown in the graph indicate that the Mn(III) corrole complex exhibits excellent pseudo-catalase activity comparable to the natural enzyme from bovine serum, which is an excellent result, in line with the objective of the study.

3.2.2. MnTexCOOH inhibition activity on BSA aggregation

One of the primary objectives of this thesis project was to investigate the inhibitory activity of MnTexCOOH toward Aβ peptides aggregation. With this goal, the texaphyrin effect was initially evaluated using Bovine Serum Albumin (BSA) as a model of amyloid aggregation.

BSA is a protein composed of 580 residues and three domains, each predominantly characterized by α-helical structures.[20]

When subjected to temperatures between 65°C and 70° C, BSA reaches a partially destabilized state, exposing many hydrophobic sites, with the following formation of aggregates rich in β-sheet motifs through disulfide bridges between cysteine residues and non-covalent interactions (Fig. 24). Under these conditions, the formation of oligomers and subsequently fibrils, is frequently used as a model comparable to the fibrils formed by Aβ peptides in aggregation studies; in both cases, a structural conversion from α-helices to β-sheets occurs, resulting in the production of insoluble aggregates.

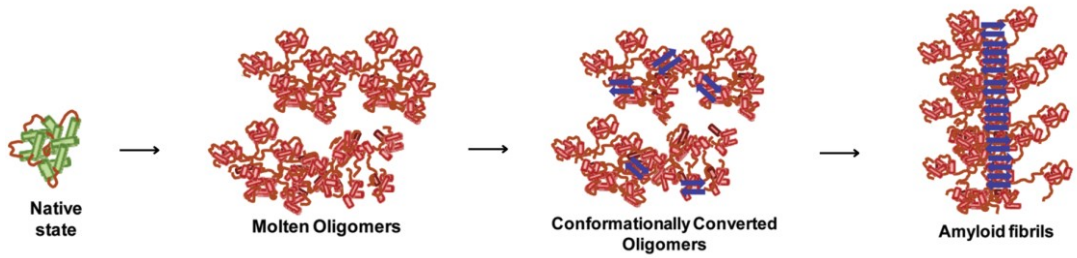

Fig. 24 *Model for fibril formation process from serum albumins.*[20]

To monitor and study the amyloid aggregation process, as in the case of the BSA protein or Aβ peptides, fluorescent dyes such as Thioflavin T (ThT) and Thioflavin S (ThS) are commonly used.[21] Although ThT is a pure compound, and ThS is a mixture, both function through the same mechanism. In solution, the molecules are free to rotate around a single C-C bond, dissipating the absorbed light energy through rotational motion. When aggregates rich in β-sheet motifs are present, the dye binds to the fibrils and its conformation is locked; the compound is no longer able to dissipate the absorbed energy through rotation, so it is instead emitted as fluorescence.

However, the main limitation of ThT and ThS is that their emission spectra frequently overlap with those of aromatic components in proteins and cellular environments. For this reason, a different fluorescent dye, ProteoStat, was employed in this study.

ProteoStat dye works, like ThT, as a rotor molecule, it shows a strong absorbance around 500 nm and maximum emission around 600 nm. These properties reduce spectral interferences previously described. Compared to other dyes, ProteoStat exhibits a brighter signal and a larger linear detection range for protein aggregation.

The dye is also used in *in vitro* studies involving bacterial cells because its structure, described in Fig. 25, allows it to pass through the double membrane characteristic of bacteria.[22]

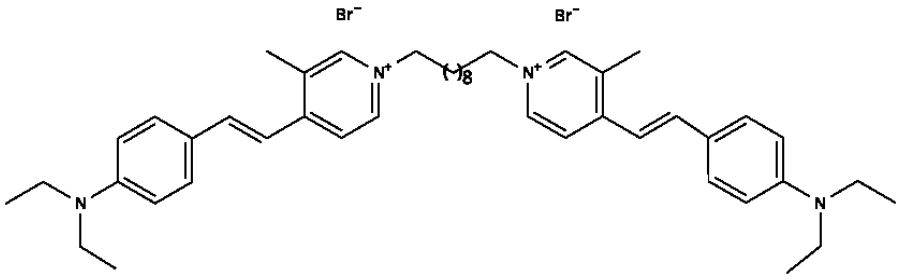

Fig. 25 *Yat ProteoStat 2150 structure.*[22]

The inhibitory activity of the MnTexCOOH complex against BSA protein aggregation was studied using spectrofluorometry. All samples were prepared containing a fixed concentration of BSA (30 μM) and ProteoStat dye (1 μM), while texaphyrin was added in increasing concentrations (3–70 μM) to the various samples; all samples were incubated for 20 hours at 65°C, the protein aggregation temperature, with stirring at 700 rpm. At the end of the incubation process, measurements were taken to determine the fluorescence intensity of the dye within each sample.

A correction was necessary because MnTexCOOH complex, due to its planar structure, replaces the ProteoStat dye at certain points within the aggregate; this phenomenon altered the measured fluorescence intensity of the samples. To correct the obtained values, an assay was conducted in which a sample containing the aggregated protein (30 μM) with only the ProteoStat dye (1 μM) was prepared. Based on this sample, a spectrofluorometric titration was performed using the texaphyrin; from the data obtained, a calibration curve was created, and the correct fluorescence value for each sample was interpolated from the line of the curve. The experimental procedure for this assay is described in paragraph 4.5.3. in “Materials and methods” chapter; in the following table the corrected fluorescence values are reported.

Sample	MnTexCOOH (μM)	Fluorescence (AU)	% Inhibition
1	1	18876	0%
2	3	17775	1%
3	5	17031	5%
4	10	16322	9%
5	15	15790	12%
6	20	14541	19%
7	25	13553	24%
8	30	11430	36%
9	40	8981	50%
10	50	7587	58%
11	60	4843	73%
12	70	4222	76%
BSA Control	0	20524	-
MnTex Control	10	2652	-

Tab. 5 *Data from the spectrofluorometric measurement of samples containing BSA (30 μM), ProteoStat dye (1 μM) and MnTexCOOH (3 – 70 μM); Control solutions with aggregated BSA alone (30 μM) and MnTexCOOH alone (10 μM), all in native buffer 50 mM pH 7,4.*

Based on the values of the control solutions, which contained only MnTexCOOH and only ProteoStat dye, respectively, it was possible to determine the percentage of inhibitory activity of the complex using the following equation[23]:

$$\%\ Inhibition = \left(1 - \frac{I - I_{MnTex}}{I_o - I_{MnTex}}\right) \cdot 100$$

In the equation I represents the fluorescence intensity of the single sample, I_{MnTex} represents the texaphyrin control solution and I_o is the aggregated protein control solution.

Based on the results of the spectrofluorometric assay, it was possible to fit the activity percentages to the respective concentrations of the added MnTexCOOH and to calculate the IC_{50} value (Fig. 26). IC_{50} is defined in literature as the Half-Maximal Inhibitory Concentration, this value indicates the exact concentration of an inhibitor (the texaphyrin in this case) required to reduce a given biological process by 50%.[24]

The equation used to calculate the IC_{50} for MnTexCOOH against BSA aggregation was the following:

$$IC_{50} = [I]\left(\frac{100 - I_{\%}}{I_{\%}}\right)^{1/h}$$

Where *I%* represents the percentage of inhibition, *[I]* indicates the corresponding concentration of texaphyrin, and *h* is the Hill coefficient, which corresponds to the slope of the curve in its linear portion.[24]

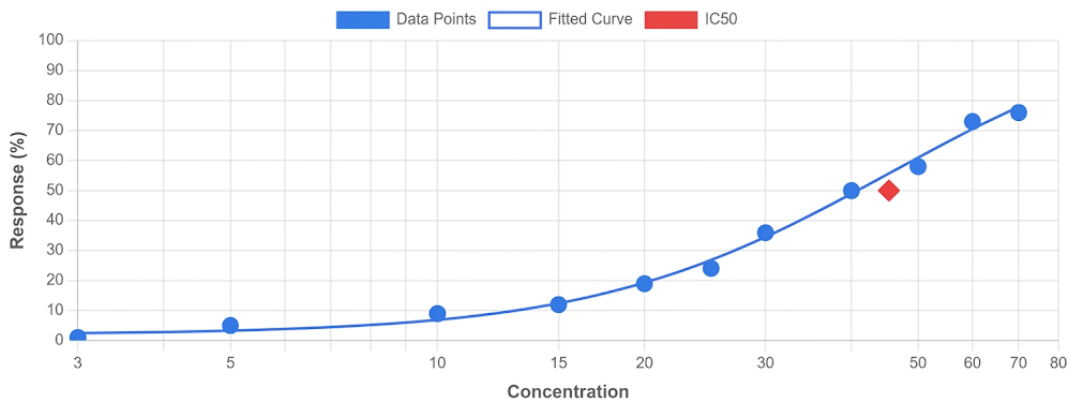

Fig. 26 *Dose-Response curve with inhibition percentage and MnTexCOOH concentration values (expressed in µM); the red square indicates the IC_{50} value.*

IC_{50} value	45,350 µM
R^2 value	0,995
Hill slope	2,019

Tab. 6 *IC_{50} value along with curve parameters.*

As a further analysis for the study of BSA aggregation, a Dynamic Light Scattering (DLS) measurement was performed; this technique allows for the determination of the hydrodynamic radius of particles or aggregates in solution based on their diffraction of light from a beam incident on the sample. The particles move through the solution in a Brownian motion; the speed of the particles is inversely proportional to their size, and as the speed changes, so does the intensity of the scattered light by the particles. Based on the intensity of the scattered light, the hydrodynamic diameter is calculated and expressed as the Z-Average.

For the measurement different samples and a control solution were prepared, containing all the same concentration of BSA (30 μM) and different concentrations of MnTexCOOH (20 and 30 μM), the samples were incubated at 65° C overnight under 700 rpm stirring.

The results obtained are shown in the following table:

Sample	Z-Average (nm)	PDI
BSA Control	613,9	0,394
BSA + MnTexCOOH 20 μM	390,9	0,683
BSA + MnTexCOOH 30 μM	267,7	0,492

Tab. 7 *Data obtained from DLS analysis showing the diameter of the aggregate (Z-average) and the polydispersity index (PDI); each sample contains a fixed concentration of BSA (30 μM) and a variable concentration of MnTexCOOH (0 – 30 μM) in native buffer 50 mm pH 7,4.*

The data obtained from DLS analysis show a clear decrease in the size of the aggregates present in the samples was observed compared with the peptide aggregates without inhibitor, indicating high inhibitory activity. Based on the results, it can be concluded that texaphyrin exhibits high inhibitory activity against BSA protein aggregation; therefore, the preliminary phase of this study proved to be an excellent starting point for investigating the same inhibitory effect on $A\beta_{40}$ peptide.

3.2.3. MnTexCOOH inhibition activity on $A\beta_{40}$ aggregation

The inhibitory activity of the MnTexCOOH complex against $A\beta_{40}$ peptide aggregation was studied using spectrofluorometry, applying the same procedure used for BSA. All samples were prepared containing a fixed concentration of $A\beta_{40}$ (30 μM) and ProteoStat dye (1 μM), while texaphyrin was added in increasing concentrations (0,25–70 μM) to the various samples.
All samples were incubated for 20 hours at 37°C, the protein aggregation temperature, with stirring at 700 rpm. At the end of the incubation process, measurements were taken to determine the fluorescence intensity of the dye within each sample. The same correction assay as BSA has been carried out to correct fluorescence intensity values; the experimental procedure is reported in paragraph 4.5.4. in “Materials and methods” chapter. Inhibition activity percentage of MnTexCOOH has been calculated using the equation previously described.

Sample	MnTexCOOH (μM)	Fluorescence (AU)	% Inhibition
1	1	19174	0%
2	2	17239	8%
3	3	13607	27%
4	5	7406	60%
5	10	5775	69%
6	15	4425	76%
7	20	4002	79%
8	25	3467	81%
9	30	2499	87%
$A\beta_{40}$ control	0	25765	-
MnTex control	10	1058	-

Tab. 8 *Data from the spectrofluorometric measurement of samples containing $A\beta_{40}$ (30 μM), ProteoStat dye (1 μM) and MnTexCOOH (1 – 30 μM); Control solutions with aggregated $A\beta_{40}$ alone (30 μM) and MnTexCOOH alone (10 μM), all in native buffer 50 mM pH 7,4.*

The IC_{50} value has been calculated, as for BSA assay, using the inhibition percetage values calculated from fluorescence intensities; the calculation has been carried out using the equation perviously described.

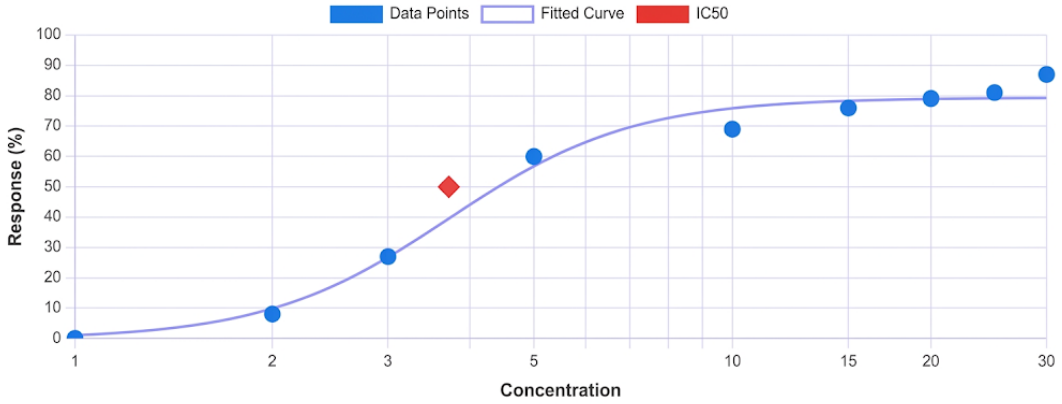

Fig. 27 *Dose-Response curve with inhibition percentage and MnTexCOOH concentration values (expressed in μM); the red square indicates the IC_{50} value.*

IC_{50} value	3,711 μM
R^2 value	0,985
Hill slope	3,113

Tab. 9 *IC_{50} value along with curve parameters.*

For the DLS analysis different samples and a control solution were prepared, containing all the same concentration of Aβ40 peptide (30 μM) and different concentrations of MnTexCOOH (2 - 30 μM), the samples were incubated at 37° C overnight under 700 rpm stirring. The results obtained are shown in the following table:

Sample	Z-Average (nm)	PDI
Aβ40 Control	802,4	0,644
Aβ40 + MnTexCOOH 2 μM	655,4	0,386
Aβ40 + MnTexCOOH 20 μM	371,9	0,479
Aβ40 + MnTexCOOH 30 μM	303,7	0,362

Tab. 10 *Data obtained from DLS analysis showing the diameter of the aggregate (Z-average) and the polydispersity index (PDI); each sample contains a fixed concentration of* Aβ40 *(30 μM) and a variable concentration of MnTexCOOH (0 - 30 μM) in native buffer 50 mm pH 7,4.*

The results obtained from DLS analysis for the inhibition study were satisfactory, a clear decrease in the size of the aggregates present in the samples was observed compared with the peptide aggregates without inhibitor, indicating high inhibitory activity.

As a final test to observe the inhibition of peptide aggregation, an Atomic Force Microscopy (AFM) measurement was performed: this technique requires the use of a sharp tip attached to a flexible cantilever which scans the sample surface, its interaction with the surface is monitored via laser beam reflected onto a position-sensitive photodiode. The instrument provides a high-resolution imaging of the sample highlighting dimensions of particles/aggregates, height profiles and surface roughness. The experiment was conducted on one sample containing Aβ40 peptide (Fig. 28) and MnTexCOOH that was previously incubated for 20 h at 37° C with 1200 rpm stirring (Fig. 29).

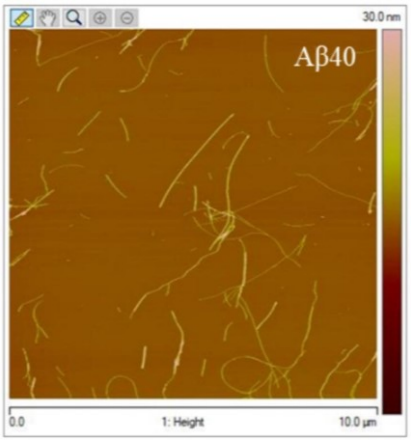

Fig. 28 *AFM image with scale 0 – 10 μm of the aggregated sample containing Aβ40* peptide alone *15 μM in native buffer 50 mM pH 7,4.* [22]

a) 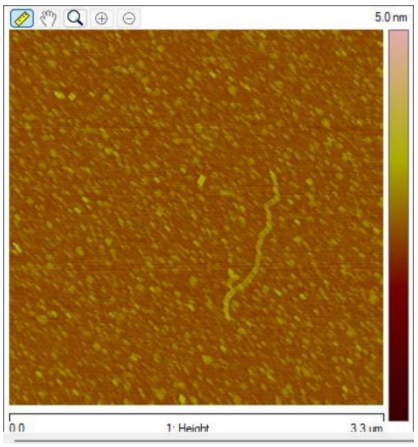

b) 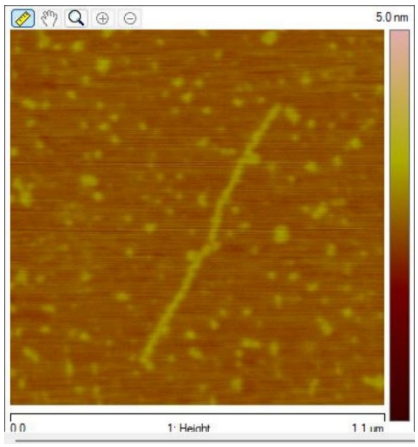

Fig. 29 *AFM images a) scale 0 – 3,3 µm, b) scale 0 – 1,1 µm of the aggregated sample containing $A\beta_{40}$ 30 µM, MnTexCOOH 2 µM in native buffer 50 mM pH 7,4.*

The images obtained shown in Fig. 29, in presence of texaphyrin, revealed a peptide aggregate smaller than 1 µm, a size significantly smaller than those reported in the literature for peptide aggregates without an inhibitor. A comparison can be made with Figure 28, which shows aggregates approximately 4 µm in length, with half of the concentration of $A\beta_{40}$ peptide, confirming a considerable reduction in amyloid fibrils in the presence of MnTexCOOH.

It can be concluded that the MnTexCOOH complex exhibits highly effective inhibitory activity against peptide aggregation. It has been hypothesized that the texaphyrin complex interacts with the N-terminal end of the $A\beta_{40}$ peptide in its monomeric form through a bond between the amino group of the terminal aspartic acid residue.

A metal-ligand bond would form between the nitrogen atom, which would act as a donor of an electron pair, and the Mn(II) ion at the center of the complex, which would be the acceptor of the electron pair; the metal ion would bind axially to the nitrogen atom, resulting in a hexacoordinate conformation. By binding the peptide in its monomeric state, the complex would prevent binding with other monomeric peptides, thereby blocking peptide aggregation and the formation of oligomers and, subsequently, insoluble fibrils.

3.2.4. MnTexCOOH inhibition activity on Aβ$_{40}$ aggregation in E. coli

A further step in the study of the inhibitory activity of the MnTexCOOH complex involves analyzing the inhibition of the Aβ$_{40}$ peptide expressed within the bacterium *Escherichia coli*. To induce the expression of a specific peptide, a process of genetic recombination must be carried out: the gene sequence encoding the peptide is inserted into a plasmid expression vector, which can be a bacterial cell as *E. coli*. The gene sequence is positioned near a sequence known as a regulatable promoter, which functions as a starting point for DNA transcription by the enzyme RNA polymerase. This system operates according to a molecular switch control mechanism based on the interaction between a repressor protein and the regulatable promoter (Fig. 30).

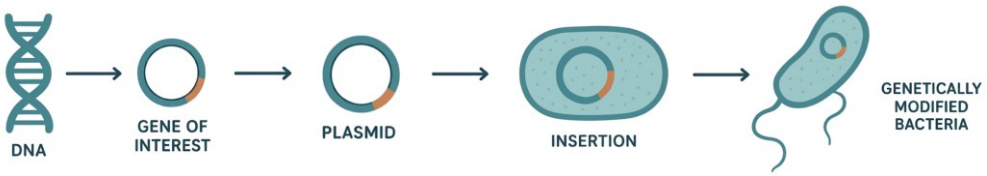

Fig. 30 *Schematic gene cloning process.*[25]

In this study, isopropyl-β-D-1-thiogalactopyranoside (IPTG), a thioglycoside, was used to regulate the expression of the peptide within the bacterium.

Without the addition of IPTG to the culture medium containing the bacteria, the repressor protein specifically binds to the promoter region, blocking the binding of RNA polymerase to the DNA strand through steric hindrance and preventing transcription from occurring. This blocks the expression of the peptide, which will therefore not be produced.

If, on the other hand, IPTG is added to the culture containing the bacteria, it penetrates the bacterial cell and binds with high affinity to the repressor protein, preventing it from binding to the promoter. In this way, the binding of RNA polymerase is not impeded; therefore, transcription and subsequently the synthesis of the peptide of interest, in this case the Aβ$_{40}$ peptide, can take place.

For this study, an experiment was conducted using a culture of *E. coli* bacteria provided by a collaborating laboratory. The first step of the experiment was to prepare a "starting medium" solution containing the nutrients needed to grow the bacterial culture. The bacteria, which had been stored at -20 °C, were added to this solution, and the mixture was incubated at 37 °C with stirring at 220 rpm overnight. The next step was to add the ProteoStat dye (so that the final concentration in the Eppendorf tube was 1 μM) and divide the starting solution into two sets of Eppendorf tubes.

IPTG was added to the first set, causing the bacteria to express the $A\beta_{40}$ peptide, while no IPTG was added to the second set, so the peptide was not produced by the bacteria.

MnTexCOOH was added to both sets of samples in increasing concentrations (0 – 30 μM), including a control solution containing only the solution with bacteria; finally, all samples were incubated at 37 °C with stirring at 220 rpm overnight to induce peptide aggregation, where applicable. At the end of the incubation, absorbance and fluorescence intensity were measured; both measurements were necessary to calculate the inhibitory activity of the complex, since the concentration of $A\beta_{40}$ peptide within the bacteria present in the samples is unknown; the inhibition percentage was calculated using the equation reported below. The experimental procedure is reported in paragraph 4.5.5. in "Materials and methods" chapter.

With IPTG

		MnTexCOOH				
	Control sol.	0,5 μM	2 μM	5 μM	15 μM	30 μM
Fluo (AU) / Abs (AU)	301172,4	239042,2	219852,6	191385,3	158515,3	98048,6
		31%	35%	44%	56%	77%

Without IPTG

		MnTexCOOH				
	Control sol.	0,5 μM	2 μM	5 μM	15 μM	30 μM
Fluo (AU) / Abs (AU)	104146,9	103399,5	90963,0	80167,9	71720,8	53142,8

Tab. 11 *Data obtained from E. coli assay; fluorescence/absorbance value is reported for each sample, this value has been used in order to calculate the percentage of inhibition activity.*

The following equation has been used to calculate MnTexCOOH inhibition activity; both absorbance and fluorescence values, in the set with and without IPTG, have been involved in the calculation.

$$\%\ Inhibition = 1 - \left(\frac{Fluo/Abs_{\ with\ IPTG+MnTex} - Fluo/Abs_{\ without\ IPTG+MnTex}}{Fluo/Abs_{\ with\ IPTG} - Fluo/Abs_{\ without\ IPTG}}\right) \cdot 100$$

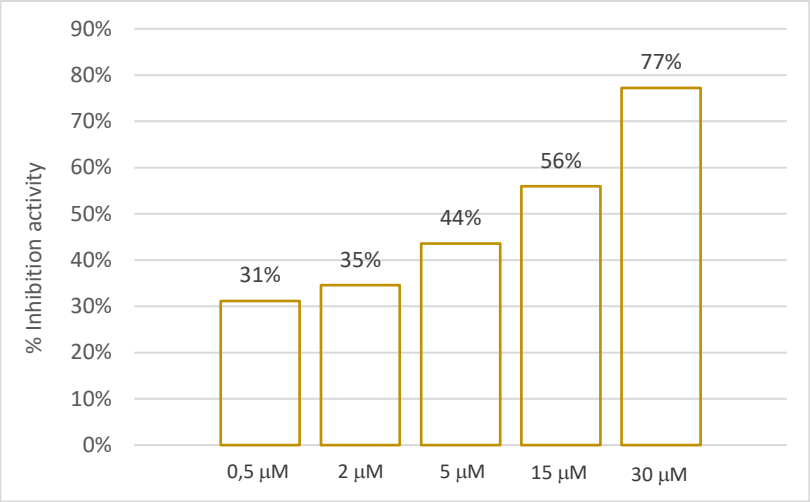

Fig. 31 *Graphic showing the percentages of inhibitory activity; the x-axis shows the concentrations of MnTexCOOH added to the respective samples.*

As can be seen from the graphic showing the results (Fig. 31), the percentages of inhibitory activity of the complex show significant values, indicating excellent inhibitory activity and also suggesting that the texaphyrin has proven capable of penetrating the bacterium where the expressed $A\beta_{40}$ peptide is located, thus crossing the double lipid membrane that protects the negative Gram bacteria. These results, however, provide only qualitative information because, since the concentration of the peptide inside the bacteria in each sample is unknown, it was not possible to correct the fluorescence intensity values, as was done for the assay not involving *E. coli*.

4. Materials and methods

4.1. Instrumentation

- UV/Vis Spectrophotometer: Agilent 8433 with a photodiode array detector, within a 190 – 1100 nm wavelength range, using 1cm pathlength quartz cuvette.
- HPLC-MS: Autosampler Surveyor IC pump (Thermo Finnigan) coupled with the Thermo Finnigan LCQ ADV MAX ion-trap mass spectrometer equipped with an ESI source. The column used was a Phenomenex Jupiter column, 4 µm, 2.0 × 150 mm, Proteo 90 Å, with a flow rate of 0.2 mL/min (Bioworks 3.1 software for data analysis).
- HPLC: Jasco LC-NET II/ADC with a photodiode array detector MD-150 MWD, within a 190 – 650 nm wavelength range.

- Zetasizer DLS: Static Light Scattering at 90° C, using M3-PALS analysis nd constant current zeta mode (particle size measurement from 0,3 nm to 10 μM).
- FLUOstar Omega: multi-mode microplate reader for absorbance and fluorescence intensity detection, with shaking system and temperature incubation system up to 65° C (Omega BMG software for data analysis).
- Bruker multimode Nanoscope IV with RTESPA-150 probes, with a nominal spring constant of 5 nN nm^{-1} and a nominal radius of 8 nm, from Bruker AFM probes. All images were processed by Bruker NanoScope Analysis Software.

4.2. Synthesis of 5,10,15-tris(p-carboxyphenil) Fe(IV) chloride corrole (FeTCPC)

The synthesis of the FeTCPC complex was performed according to a procedure described in the literature, with some minor modifications applied to certain steps.[26]

The ligand was synthesized (Fig. 32) by dissolving methyl p-formylbenzoate (5 mmol, 821 mg) in MeOH (200 mL), followed by the addition of pyrrole (10 mmol, 697 μL) in water (200 mL) and subsequently 4.25 mL of concentrated HCl (6 M). The mixture was left stirring for 3 hours.

An extraction was carried out using a separatory funnel with $CHCl_3$; the organic phase was washed with distilled water (3 times) and then dried over Na_2SO_4. Finally, the mixture was filtered, and the product was diluted with 300 mL of $CHCl_3$.

The macrocycle was oxidized by adding p-chloranil (5 mmol, 1.23 g) and refluxed for 2 hours. Upon completion of the reaction, the solvent was removed using a rotary evaporator. Purification was performed by HPLC (semi-preparative silica-packed column) using a DCM/CH_3 linear gradient.

The product (bright green) in DCM exhibited the following UV-Vis maximum absorption: 430, 590, and 638 nm, and ESI-MS peak: m/z = 701(+).

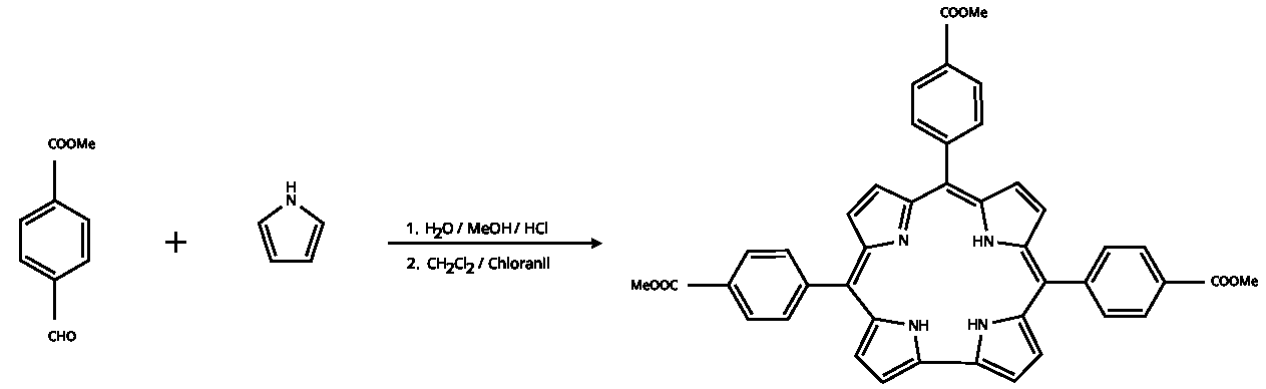

Fig. 32 *Synthesis reaction of H_3TCMPC ligand.*

The H_3TCMPC ligand (68 mg, $9.7 \cdot 10^{-5}$ mol) was dissolved in argon saturated DMF (5 mL total). Anhydrous $FeCl_2$ (247 mg, $1.94 \cdot 10^{-3}$ mol) in DMF was subsequently added, and the reaction mixture was refluxed under an inert atmosphere for 2 hours in the dark (Fig. 33).

The resulting solution was cooled to room temperature, and HCl (3 M, 1.82 mL in 20 mL of solution) was added dropwise to induce product precipitation. The suspension was centrifuged, and the supernatant was discarded. The precipitate was dissolved in an excess of DCM (100 mL) and extracted with 7% HCl (21 mL in 300 mL of solution) (this process is repeated 3 times).

The organic phase was dried over Na_2SO_4, filtered, and concentrated under reduced pressure using a rotary evaporator. The crude product was further purified by silica gel column chromatography, eluting initially with an EtOAc/Hexane mixture (4:1, v/v) until a light pink-brown spot was eluted. The eluent was then switched to a $CHCl_3$/MeOH mixture (9:1, v/v) to collect a major green-brown spot. Finally, the solvent was evaporated from the collected fraction.

The product (brown) in DCM exhibited the following UV-Vis maximum absorption: 364, 408, 640 nm, and ESI-MS peak: m/z = 753(+).

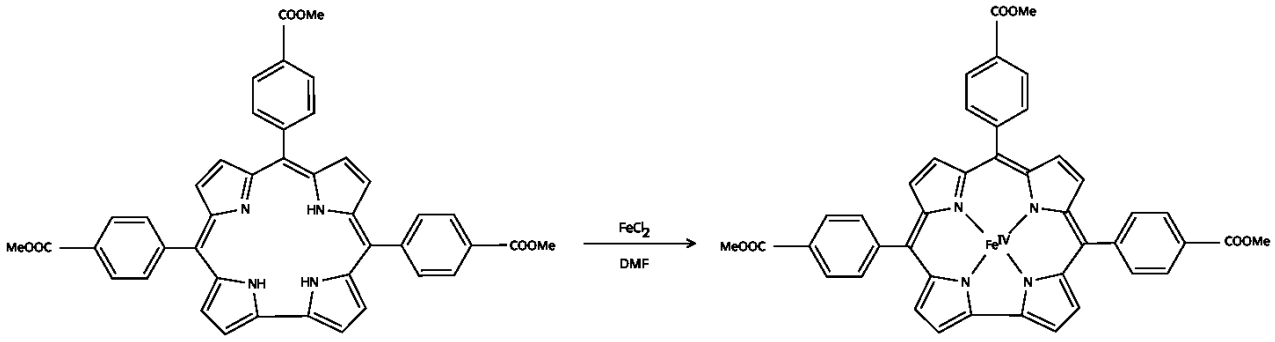

Fig. 33 *Metalation reaction with formation of FeTCMPC complex.*

For the deprotection of the carboxylic groups (Fig. 34), the FeTCMPC complex (10 mg) was dissolved in THF (5 mL). A mixture of MeOH (5 mL) and KOH (220 mg in 1.5 mL of H_2O) was added dropwise very slowly under vigorous stirring. The reaction mixture was kept at 40 °C in the dark for 24 hours. Upon completion of the reaction, the mixture was cooled to room temperature and acidified with HCl (6 M) to a pH of approximately 3. Subsequently, DCM was added, the organic layer was washed with water, and the solvent was removed using a rotary evaporator. The product (brown) in Acetone exhibited the following UV-Vis maximum absorption: 364, 408, 640 nm, and ESI-MS peak: m/z = 711(+).

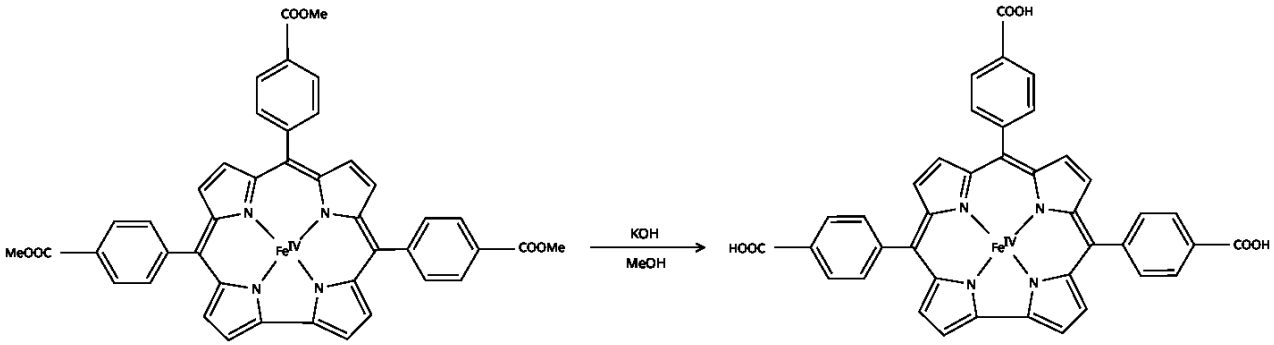

Fig. 34 *Hydrolysis reaction with formation of FeTCPC complex.*

4.3. Synthesis of 5,10,15-tris(4-pyridil) Mn(II) corrole (MeMnTPC)

The synthesis of the MeMnTPC complex was performed according to a procedure described in the literature, with some slight modifications applied to certain steps of the process.[15]

To synthesize the ligand (Fig. 35), pyrrole (60.5 mmol – 4.2 mL) and 4-pyridinecarboxaldehyde (20.2 mmol – 1.93 mL) are dissolved in 250 mL of acetic acid, the reaction is refluxed for 4 hours. Once the reaction is complete, the mixture cooled to room temperature, and the solvent is removed via rotary evaporation.

Purification is carried out through two chromatographic separations: for the first column, packed with silica gel, a CH_2Cl_2/MeOH (8.5:2) eluent mixture is used, and the first green spot is collected. For the second column, also packed with silica gel, an EtOAC/MeOH (96: 4) eluent mixture is used. The second green spot is collected; then, the product is concentrated with rotary evaporator.

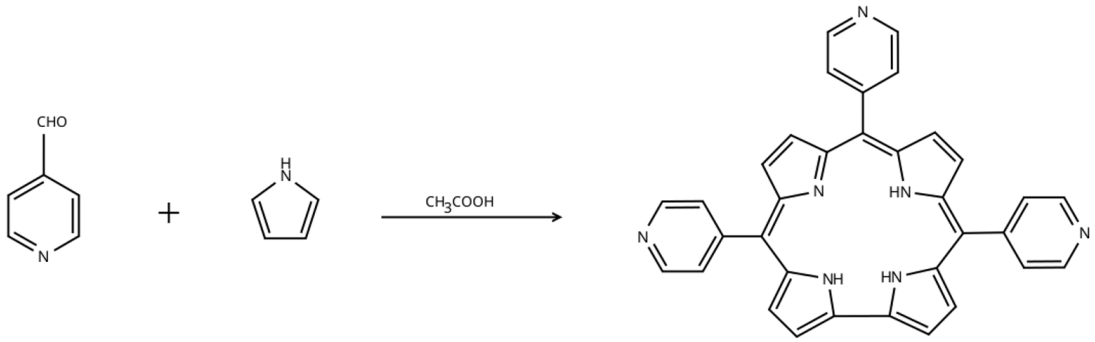

Fig. 35 *Synthesis reaction of H_3TPC ligand.*

To synthesize the complex, the ligand (38 mg) is dissolved in 20 mL of pyridine; then, the salt $(CH_3COO)_2Mn\ 4H_2O$ (10 eq) is added (Fig. 36). The reaction mixture is stirred at 60 °C for 1 hour. In the end, the solvent is removed using a rotary evaporator. The product showed an ESI-MS peak at m/z = 582(+).

For the purification step the dry product was dissolved in an EtOAc/MeOH (5:1) mixture and purified by column chromatography packed with neutral alumina (deactivated with 10% w/w water), using an EtOAc/MeOH eluent mixture starting at 5:1 and subsequently increased to 2:1. The product was collected as a green spot. Lastly, the solvent was removed with rotary evaporation.

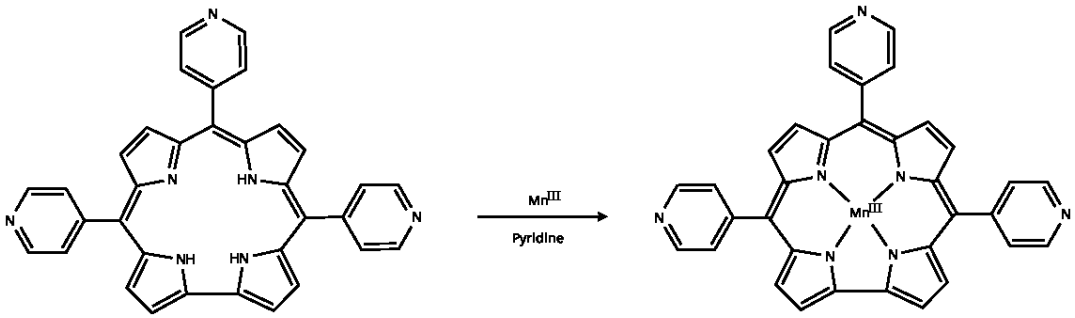

Fig. 36 *Metallation reaction with formation of MnTPC complex.*

Methylation of the MnTPC Complex:

Under inert atmosphere, the MnTPC complex (1 eq.) is dissolved in DMF (5 mL), then Methyl iodide (5 eq.) is added to the solution (Fig. 37). The reaction mixture is heated in an oil bath at 35 °C for 16–18 hours. The reaction is monitored by TLC using alumina plates (mixture of Chloroform, 1% v/v in MeOH).

If the starting material is not completely converted, some more methyl iodide is added, then the mixture is kept under stirring until complete disappearance of the starting material. Once the reaction is complete (light brown product), the solvent is removed using a rotary evaporator. The product (brown) in MeOH exhibited the following UV-Vis maximum absorption: 308, 435, 645 nm, and ESI-MS peak: m/z = 711(+).

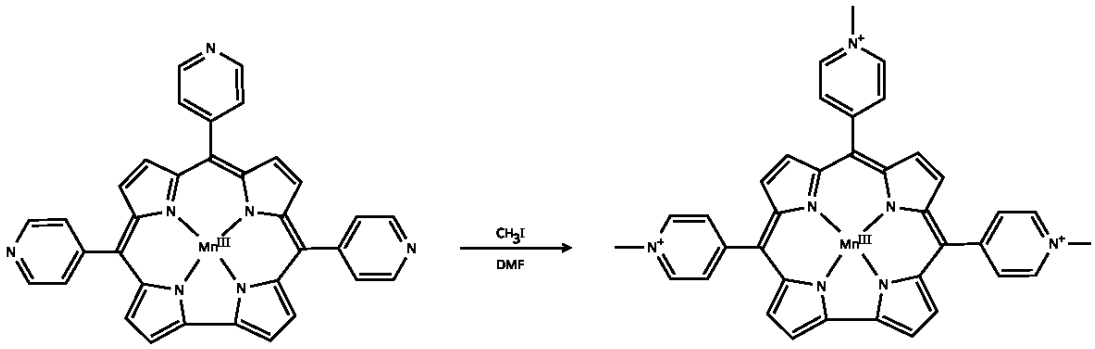

Fig. 37 *Metilation reaction with formation of MeMnTPC complex.*

4.4. Characterization of MnTexCOOH

MnTexCOOH solution concentration was determined by weighing the solid compound (MW = 764,7 g/mol), the stock solution was prepared in MeOH and subsequently diluted in MeOH. The molar extinction coefficient in MeOH was determined through a spectrophotometric titration with incremental additions of a 18,8 μM MnTexCOOH solution, the absorbance was monitored at 452 nm (Fig. 38).

Additions (μL)	Total vol. (μL)	MnTex (μM)	Abs (450 nm) (AU)
0	2000	0,000	0
2	2002	0,100	$7{,}68 \times 10^{-3}$
2	2004	0,200	$1{,}42 \times 10^{-2}$
2	2006	0,299	$1{,}97 \times 10^{-2}$
2	2008	0,398	$2{,}59 \times 10^{-2}$
2	2010	0,498	$3{,}14 \times 10^{-2}$
2	2012	0,596	$3{,}85 \times 10^{-2}$
2	2014	0,695	$4{,}49 \times 10^{-2}$
2	2016	0,794	$4{,}96 \times 10^{-2}$
2	2018	0,892	$5{,}67 \times 10^{-2}$

Tab. 12 *Spectrophotometric titration data of MnTexCOOH in MeOH.*

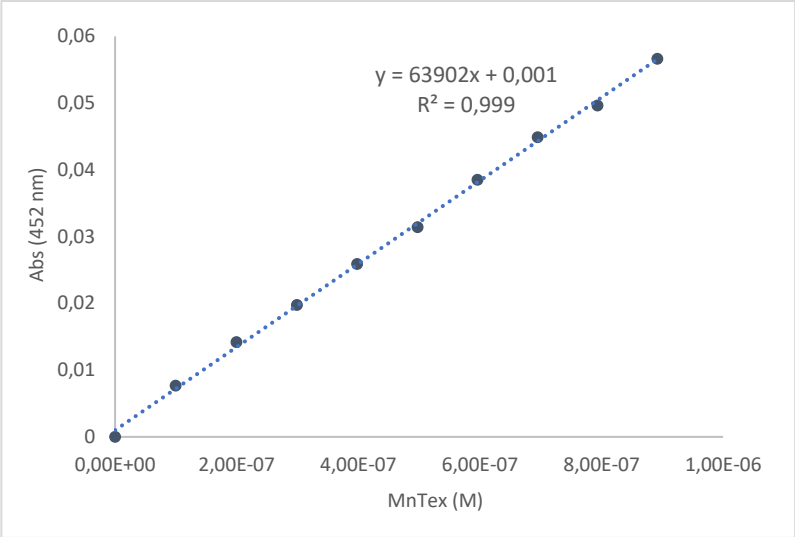

Fig. 38 *MnTexCOOH calibration line in MeOH.*

$$\varepsilon \text{ (in MeOH)} = 63902{,}621 \pm 0{,}001 \text{ M}^{-1} \text{ cm}^{-1}$$

Molar extinction coefficient in native buffer (NB) (50 mM Tris·HCl, 150 mM NaCl at pH 7.4) was determined through a spectrophotometric titration with incremental additions of a 114,7 µM MnTexCOOH solution to a native buffer starting solution, the absorbance was monitored at 450 nm, the Soret band's wavelength (Fig. 39).

Additions (µL)	Total vol (µL)	MnTex (µM)	Abs (450 nm) (AU)
0	98	0	0
2	100	2,29	0,081
2	104	4,41	0,119
2	106	6,49	0,214
2	108	8,50	0,269
2	110	10,43	0,333
2	112	12,29	0,410
2	114	14,09	0,459
2	116	15,82	0,508
2	120	19,12	0,575
2	122	20,68	0,626

Tab. 13 *Spectrophotometric titration data of MnTexCOOH in NB.*

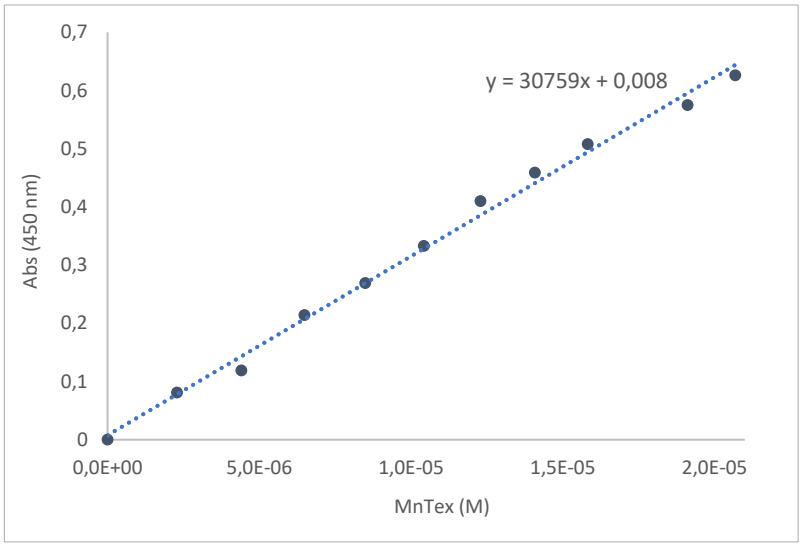

Fig. 39 *MnTexCOOH calibration line in NB.*

ε (in native buffer) = 30759,330 ± 0,008 M^{-1} cm^{-1}

4.5. Hemochromogen assay

The first step of the procedure was the preparation of a hemin solution in distilled water in a concentration corresponding to an absorbance value of 1 at 390 nm, in a quartz cuvette with a pathlenght of 1 cm (volume of the cuvette = 1600 µL). The UV-Vis spectrum was then recorded to establish the precise absorbance value at the maximum absorption of the Soret band A_{max}.

Upon the addition of 320 µL of pyridine (final concentration 0.1 M), 75 µL of 2 M NaOH (final concentration 0.075 M), and a spatula tip of Na_2SO_4 the heme-bis-pyridine adduct was formed, for which the molar extinction coefficient at 556 nm is known ε (556 nm) = 34400 M^{-1} cm^{-1}.

The UV-Vis spectrum of the solution was subsequently recorded to determine the absorbance value at 556 nm, which was then used to calculate the concentration of the heme-bis-pyridine adduct via the Beer-Lambert law. This concentration corresponds to the heme concentration in the final volume of 1,995 µL. Based on this value, the concentration of the complex in the initial volume was calculated, and by knowing the A_{max} value, the molar extinction coefficient was determined.

$$[Heme]_f = [Adduct] = \frac{A_{556\,nm}}{\varepsilon_{556\,nm}}$$

$$[Heme]_i = [Heme]_f \cdot \frac{1995\ \mu L}{1660\ \mu L}$$

$$\varepsilon_{\max Soret} = \frac{A_{\max Soret}}{[Heme]_i}$$

$$\varepsilon_{Hemin} = 67400\ M^{-1}cm^{-1}$$

4.5. Reactivity studies

4.5.2. Peroxidase-like activity of FeTCPC

The FeTCPC solution was prepared by dissolving ~2–3 mg (MW = 711 g/mol) in 1 mL of MeOH. The concentration of the hemin solution was determined by UV-Vis spectroscopy: after measuring the absorbance at 400 nm of the characteristic Soret band of the complex, the concentration was calculated using the Beer-Lambert law (molar extinction coefficient used: 35000 M^{-1} cm^{-1}).[14]

The blank for the quantification of the FeTCPC solution was recorded in MeOH, whereas the blank for kinetic studies was recorded in 20 mM phosphate buffer (pH 7,4). The quartz cuvette used (1 cm pathlength) was washed with distilled water and NaOH 1 M solutions in between measurements. Each study has been performed with two steps: the first experiment was performed with increasing concentrations of H_2O_2 and a stable concentration of substrate, in order to determine and the k_1 value of the first reaction of the catalytic cycle, from the initial slope at low H_2O_2 concentrations of the constructed curve. Subsequently, higher concentrations were observed to determine the maximum value corresponding to the saturating peroxide concentration.

The second experiment was performed in saturating conditions of H_2O_2, increasing the concentration of the substrate forming a Michaelis-Menten curve, which was fitted using the FPWIN software to determine K_M and k_{cat} values. Each study has been performed with FeTCPC and Hemin as a control and with two different substrates (3-(4-Hydroxyphenyl)propanoic acid (HPA) and 4-Methylcathecol).

4.5.2.1. HPA

HPA was the first substrate used to study the peroxidase-like activity of FeTCPC. In the presence of an oxidizing agent such as a redox-active metal, HPA generates radical intermediates that dimerize to produce a complex absorbing at 300 nm. Consequently, the reaction kinetics were monitored at this wavelength (ε = 1950 M^{-1} cm^{-1}).[1]

HPA solution for this assay has been prepared dissolving solid substrate in 100 µL of MeOH and 900 µL of milliQ water; all the measurements have been carried out in phosphate buffer 20 mM at pH 7,4.

Dependence on H_2O_2 concentration

– Hemin

Hemin (µM)	HPA (mM)	H_2O_2 (mM)	Cuvette volume (µL)
2	3	1-75	1600

H_2O_2 (mM)	v (Abs/s)	v (s^{-1})
1	$5{,}18 \times 10^{-4}$	0,133
2	$9{,}29 \times 10^{-4}$	0,238
3	$1{,}21 \times 10^{-3}$	0,311
5	$1{,}81 \times 10^{-3}$	0,464
10	$3{,}38 \times 10^{-3}$	0,868
25	$4{,}70 \times 10^{-3}$	1,205
40	$7{,}01 \times 10^{-3}$	1,797
50	$6{,}83 \times 10^{-3}$	1,750
65	$1{,}38 \times 10^{-2}$	3,538
75	$9{,}12 \times 10^{-2}$	2,338

Tab. 14 *Data obtained from the kinetic study with hemin, HPA and H_2O_2 under peroxide-dependent conditions.*

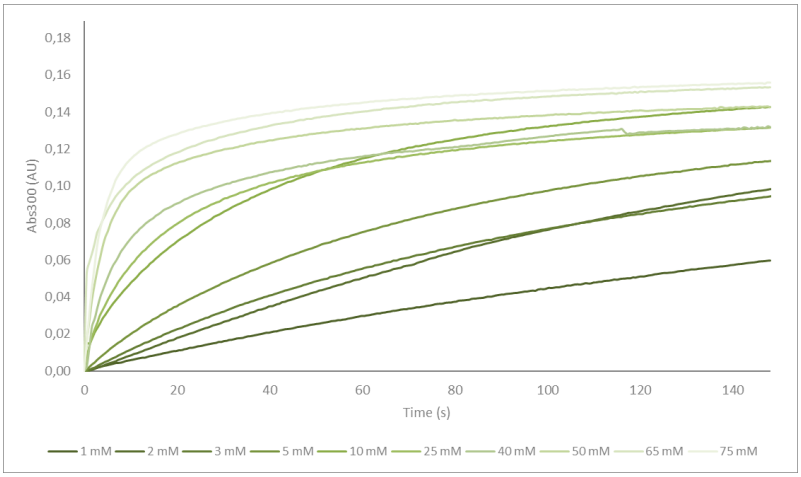

Fig. 40 *Kinetic curves of the oxidation reaction of the HPA substrate (3 mM) in presence of hemin (2 µM) and increasing concentration of H_2O_2 (1 to 75 mM) in phosphate buffer 20 mM pH 7,4.*

– FeTCPC

FeTCPC (µM)	HPA (mM)	H_2O_2 (mM)	Cuvette volume (µL)
2	3	1 - 40	1600

H_2O_2 (mM)	v (Abs/s)	v (s^{-1})
1	$1{,}25 \times 10^{-3}$	0,32
2	$1{,}69 \times 10^{-3}$	0,43
3	$2{,}11 \times 10^{-3}$	0,54
5	$2{,}65 \times 10^{-3}$	0,68
10	$3{,}79 \times 10^{-3}$	0,97
20	$5{,}29 \times 10^{-3}$	1,36
35	$4{,}36 \times 10^{-3}$	1,12
40	$4{,}02 \times 10^{-3}$	1,03

Tab. 15 *Data obtained from the kinetic study with FeTCPC, HPA and H_2O_2 under peroxide-dependent conditions.*

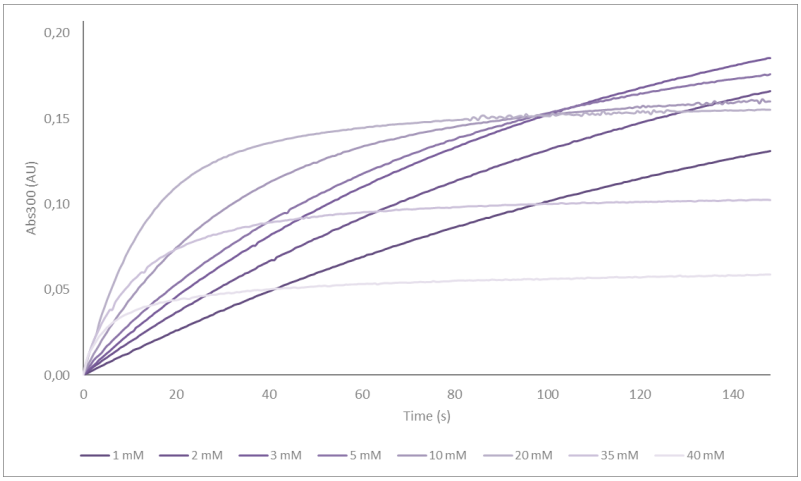

Fig. 41 *Kinetic curves of the oxidation reaction of the HPA substrate (3 mM) in presence of FeTCPC (2 µM) and increasing concentration of H_2O_2 (1 to 40 mM) in phosphate buffer 20 mM pH 7,4.*

Dependence on substrate concentration

– Hemin

Hemin (µM)	HPA (mM)	H_2O_2 (mM)	Cuvette volume (µL)
2	0,3 – 3,5	40	1600

HPA (mM)	v (Abs/s)	v (s^{-1})
0,1	3,52 x 10^{-3}	0,90
0,2	4,67 x 10^{-3}	1,20
0,5	5,36 x 10^{-3}	1,37
0,7	6,34 x 10^{-3}	1,62
1	8,14 x 10^{-3}	2,09
2	1,01 x 10^{-2}	2,60
2,5	8,80 x 10^{-3}	2,26
3	1,68 x 10^{-2}	4,30
3,5	1,20 x 10^{-2}	3,07
4	8,55 x 10^{-3}	2,19

Tab. 16 *Data obtained from the kinetic study with hemin, HPA and H_2O_2 under substrate-dependent conditions.*

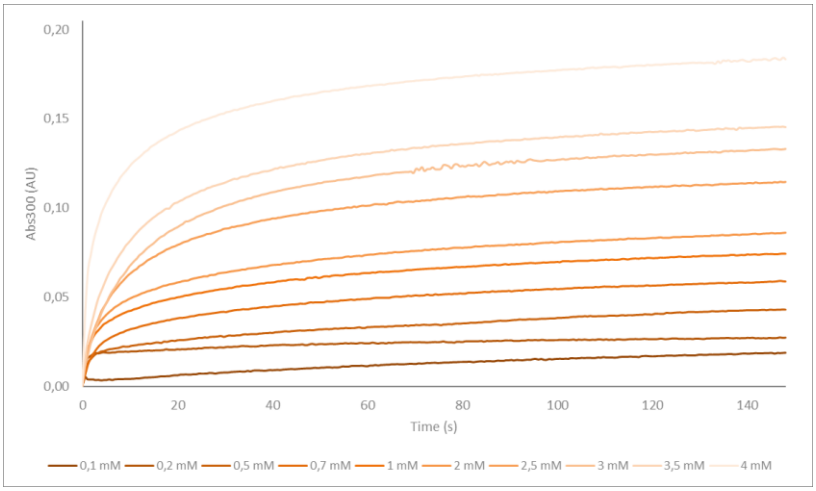

Fig. 42 *Kinetic curves of the oxidation reaction of the HPA substrate in increasing concentrations (0,3 to 3,5 mM) in presence of hemin (2 µM) and H_2O_2 (40 mM) in phosphate buffer 20 mM pH 7,4.*

– FeTCPC

FeTCPC (μM)	HPA (mM)	H_2O_2 (mM)	Cuvette volume (μL)
2	0,2 – 3,5	20	1600

HPA (mM)	v (Abs/s)	v (s^{-1})
0,2	$6,93 \times 10^{-4}$	0,18
0,5	$2,04 \times 10^{-3}$	0,52
0,7	$2,80 \times 10^{-3}$	0,72
1	$5,20 \times 10^{-3}$	1,33
1,5	$6,13 \times 10^{-3}$	1,57
2	$5,43 \times 10^{-3}$	1,39
3	$7,33 \times 10^{-3}$	1,88
3,5	$7,50 \times 10^{-3}$	1,92

Tab. 17 *Data obtained from the kinetic study with FeTCPC, HPA and H_2O_2 under substrate-dependent conditions.*

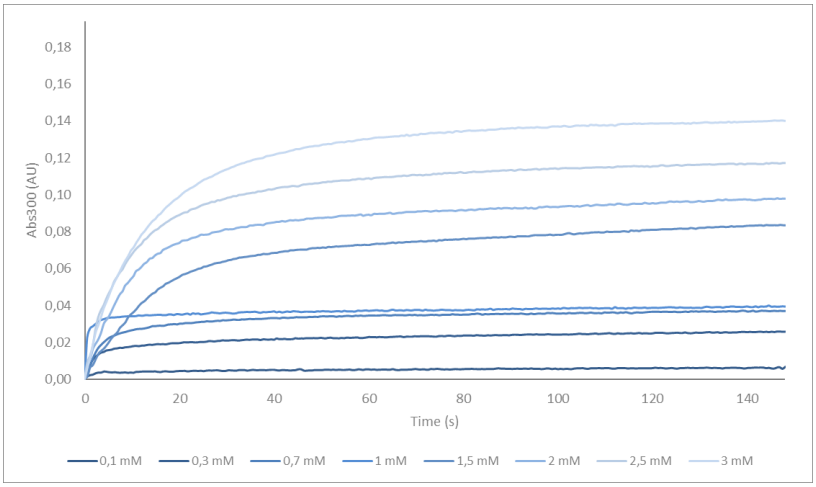

Fig. 43 *Kinetic curves of the oxidation reaction of the HPA substrate in increasing concentrations (0,2 to 3,5 mM) in presence of FeTCPC (2 μM) and H_2O_2 (20 mM) in phosphate buffer 20 mM pH 7,4.*

4.5.2.2. 4-Methylcathecol

In the presence of an oxidizing agent such as a redox-active metal, 4-methylcatechol (4-MC) is oxidized to 4-methylquinone, a species exhibiting strong absorbance near 400 nm. Accordingly, the kinetic study was performed at 400 nm (ε = 1550 M^{-1} cm^{-1}) with a baseline correction applied at 800 nm.[27] 4-MC solution for this assay has been prepared dissolving solid substrate in 1 mL of milliQ water; all the measurements have been carried out in phosphate buffer 20 mM at pH 7,4.

Dependence on H_2O_2 concentration

– Hemin

Hemin (µM)	4-MC (mM)	H_2O_2 (mM)	Cuvette volume (µL)
0,2	1	1-400	1600

H_2O_2 (mM)	v (Abs/s)	v (s^{-1})
1	1,27 x 10^{-4}	0,41
3	1,74 x 10^{-4}	0,56
5	3,88 x 10^{-4}	1,25
10	4,27 x 10^{-4}	1,38
25	1,24 x 10^{-3}	4,01
50	2,11 x 10^{-3}	6,79
100	2,34 x 10^{-3}	7,53
200	3,04 x 10^{-3}	9,79
300	3,98 x 10^{-3}	12,83
400	4,66 x 10^{-3}	15,03

Tab. 18 *Data obtained from the kinetic study with hemin, 4-MC and H_2O_2 under peroxide-dependent conditions.*

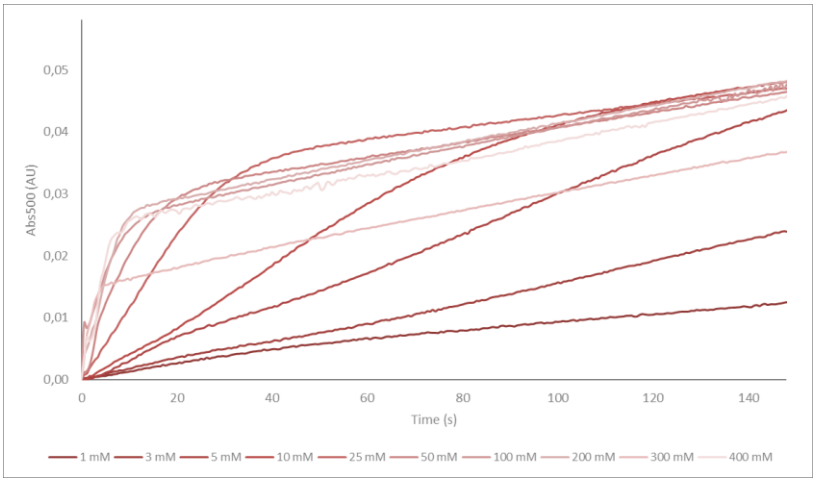

Fig. 44 *Kinetic curves of the oxidation reaction of the 4-MC substrate (1 mM) in presence of hemin (2 µM) and increasing concentration of H_2O_2 (1 to 400 mM) in phosphate buffer 20 mM pH 7,4.*

– FeTCPC

FeTCPC (µM)	4-MC (mM)	H_2O_2 (mM)	Cuvette volume (µL)
0,2	1	1-300	1600

H_2O_2 (mM)	v (Abs/s)	v (s^{-1})
1	$4{,}63 \times 10^{-4}$	1,49
3	$7{,}36 \times 10^{-3}$	2,38
5	$9{,}46 \times 10^{-4}$	3,05
15	$1{,}95 \times 10^{-3}$	6,29
25	$5{,}18 \times 10^{-3}$	16,71
50	$6{,}37 \times 10^{-3}$	20,53
75	$9{,}31 \times 10^{-3}$	30,05
150	$1{,}22 \times 10^{-2}$	39,36
200	$1{,}29 \times 10^{-2}$	41,68
250	$1{,}35 \times 10^{-2}$	43,55
300	$1{,}45 \times 10^{-2}$	46,77

Tab. 19 *Data obtained from the kinetic study with FeTCPC, 4-MC and H_2O_2 under peroxide-dependent conditions.*

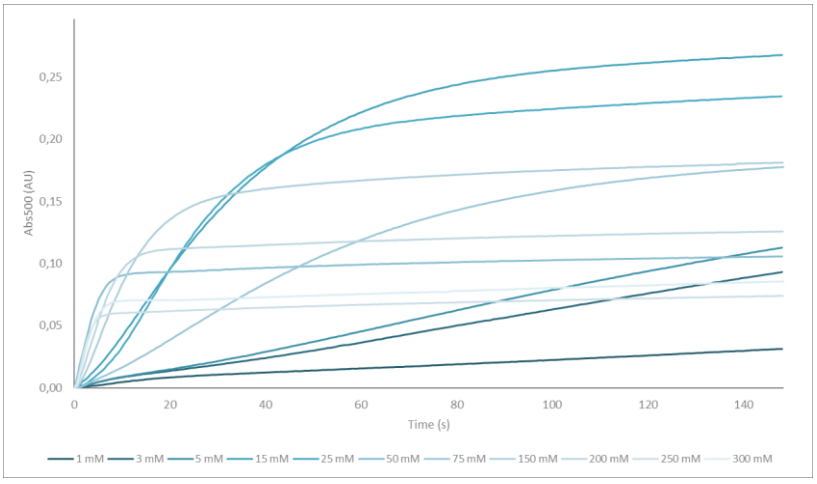

Fig. 45 *Kinetic curves of the oxidation reaction of the 4-MC substrate (1 mM) in presence of FeTCPC (2 µM) and increasing concentration of H_2O_2 (1 to 300 mM) in phosphate buffer 20 mM pH 7,4.*

Dependence on substrate concentration

- Hemin

Hemin (μM)	4-MC (mM)	H_2O_2 (mM)	Cuvette volume (μL)
0,2	0,1 - 3	400	1600

4-MC (mM)	v (Abs/s)	v (s^{-1})
0,1	2,08 x 10^{-3}	6,717
0,3	2,08 x 10^{-3}	9,615
0,6	4,39 x 10^{-3}	14,15
1	4,67 x 10^{-3}	15,055
1,5	4,88 x 10^{-3}	15,742
2	4,05 x 10^{-3}	13,078
2,5	5,14 x 10^{-3}	16,584
3	4,80 x 10^{-3}	15,471

Tab. 20 *Data obtained from the kinetic study with hemin, 4-MC and H_2O_2 under substrate-dependent conditions.*

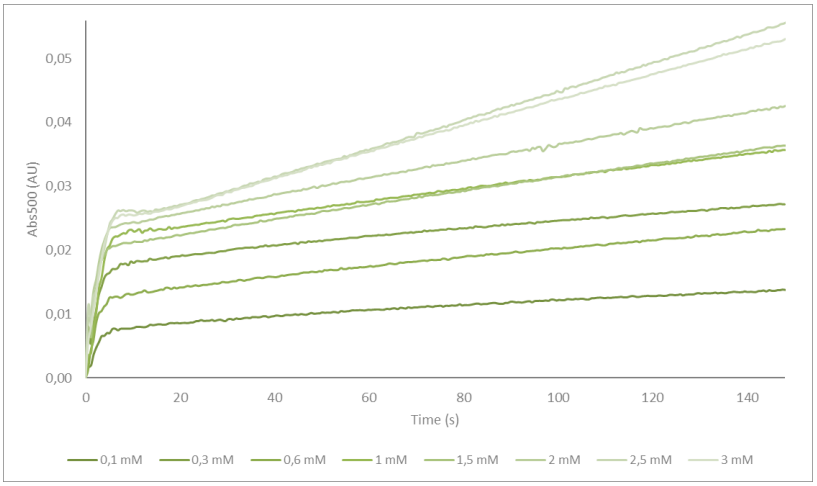

Fig. 46 *Kinetic curves of the oxidation reaction of 4-MC substrate in increasing concentrations (0,1 - 3 mM) in presence of hemin (2 μM) and H_2O_2 (400 mM) in phosphate buffer 20 mM pH 7,4.*

– FeTCPC

FeTCPC (μM)	4-MC (mM)	H_2O_2 (mM)	Cuvette volume (μL)
0,2	0,1 - 3	250	1600

4-MC (mM)	v (Abs/s)	v (s^{-1})
0,1	5,44 x 10^{-3}	17,56
0,2	1,05 x 10^{-2}	33,56
0,3	1,04 x 10^{-2}	45,65
0,5	1,42 x 10^{-2}	49,56
1	1,54 x 10^{-2}	60,76
1,5	1,88 x 10^{-2}	66,94
2	2,08 x 10^{-2}	58,47
2,5	1,81 x 10^{-2}	59,35
3	1,84 x 10^{-2}	17,56

Tab. 21 *Data obtained from the kinetic study with FeTCPC, 4-MC and H_2O_2 under substrate-dependent conditions.*

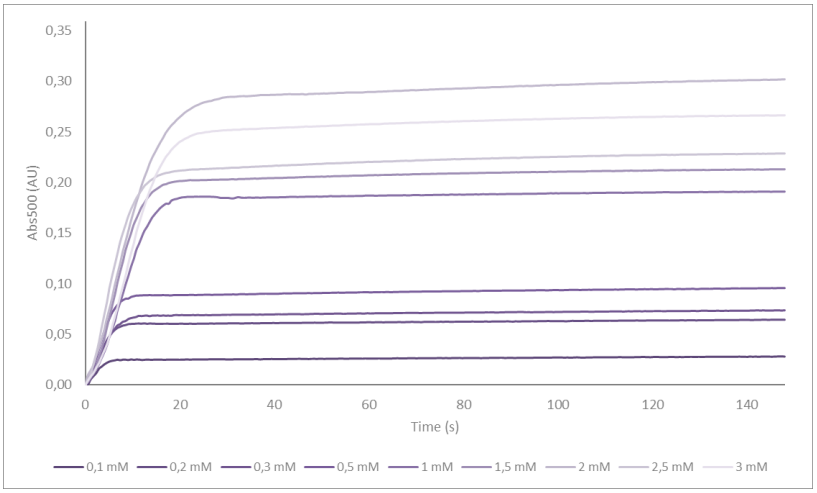

Fig. 47 *Kinetic curves of the oxidation reaction of 4-MC substrate in increasing concentrations (0,1 - 3 mM) in presence of hemin (2 μM) and H_2O_2 (250 mM) in phosphate buffer 20 mM pH 7,4.*

4.5.3. Catalase-like activity of MeMnTPC

MeMnTPC solution was prepared dissolving ~1 mg in 1 mL of MeOH, the blank was recorded in phosphate buffer 20 mM (pH 7,4). The quartz cuvette used (1 cm pathlength) was washed with distilled water and NaOH 1 M solution in between measurements.

In order to study and analyze catalase-like activity of MeMnTPC compound, a kinetic study was performed, monitoring the oxidation reaction of ABTS (2,2′-azino-bis(3-ethylbenzothiazoline-6-sulfonic acid)) catalyzed by horse radish peroxidase (HRP) in presence of H_2O_2 and phosphate buffer 20 mM pH 7,4. During this reaction ABTS is converted into his radical form $ABTS^{\bullet+}$ which absorbs at 660 nm. The kinetic study is performed following the absorbance at this wavelength for 300 seconds. ABTS, HRP and H_2O_2 solutions were prepared in milliQ water in the following concentrations:

H_2O_2 (mM)	Cat. (μM)	MnTPCMe (μM)	ABTS (mM)	HRP (μM)	Tot. volume (μL)
5	0,1	1	0,1	0,04	1600

As the first step of the kinetic study, in the cuvette phosphate buffer, H_2O_2 and MnTPCMe (or bovine catalase as a control) were incubated for 10 minutes, then ABTS and HRP were added and the measurement was immediately started.

4.5.4. MnTexCOOH inhibition activity on BSA aggregation

To study the inhibitory activity of the MnTexCOOH complex against amyloid aggregates formed by bovine serum albumin (BSA) a fluorescence emission kinetic study was performed using the fluorescent dye Yat ProteoStat.

A plate was prepared with a control solution containing only BSA at a concentration of 30 μM a control solution containing only MnTexCOOH at a concentration of 10 μM, both in native buffer. Subsequently, eight solutions containing increasing concentrations of MnTexCOOH and a constant BSA concentration of 30 μM were prepared, also in native buffer. The ProteoStat dye was added at a concentration of 1 μM to all control and sample solutions. The kinetics were carried out at 65 °C (the aggregation temperature of BSA) for 20 hours under agitation at 700 rpm. Once the measurement ended, each sample was mixed with a micropipette and reinserted into the instrument to measure the fluorescence emission value, defined as the “End point”.

From this value, along with those of the two control solutions, the percentage of protein aggregation inhibition by the texaphyrin was calculated using the following equation from literature[23] :

$$\% \, Inhibition = \left(1 - \frac{I - I_{MnTex}}{I_o - I_{MnTex}}\right) \cdot 100$$

Where I represents the fluorescence intensity of the individual sample, I_{MnTex} is the intensity of the control solution containing only MnTexCOOH, and I_o corresponds to the control solution containing only the protein.

The ProteoStat dye binds to the hydrophobic pockets formed upon protein aggregation. Initially, it was hypothesized that a portion of the dye bound to the aggregate could be displaced and replaced by the texaphyrin, thereby distorting the dye emission and, consequently, the calculated percentage of inhibitory activity.

To address this issue, an assay was carried out starting with a solution containing 30 μM protein and 1 μM dye, which was aggregated overnight at 65 °C with shaking at 700 rpm. Increasing amounts of texaphyrin were then added to this solution (1μL each), and the fluorescence intensity of the sample was measured after each addition, along with a control solution containing Proteostat 1 μM alone. The texaphyrin partially replaces the dye bound to the aggregates, lowering the fluorescence signal without this reflecting a true decrease in protein aggregation.

From these data points a calibration curve was constructed and an equation was derived; via graph interpolation it was possible to calculate the fluorescence values corresponding to the texaphyrin concentrations used in the first experiment. This equation was used to calculate the fraction value and subsequently to correct the initial fluorescence intensity values, which, after correction, resulted in higher intensity values and a slightly lower percentage of inhibition.

Additions	MnTex (μM)	Fluorescence (AU)	Fraction
0	0	21,229	1,000
1	1,0	14,871	0,687
2	2,0	13,069	0,598
3	3,0	12,154	0,553
4	3,9	10,635	0,478
5	4,8	9,866	0,440
6	5,6	9,507	0,422
7	6,4	9,440	0,419
8	7,2	8,878	0,391

9	8,0	8,661	0,381
10	8,7	8,119	0,354
11	9,4	7,774	0,337
12	10,7	7,471	0,322
13	12,0	7,042	0,301
14	13,2	6,759	0,287
15	14,3	6,338	0,266
16	15,3	5,663	0,233

Tab. 22 *Spectrophotometric titration data of MnTexCOOH with aggregated BSA and Proteostat dye.*

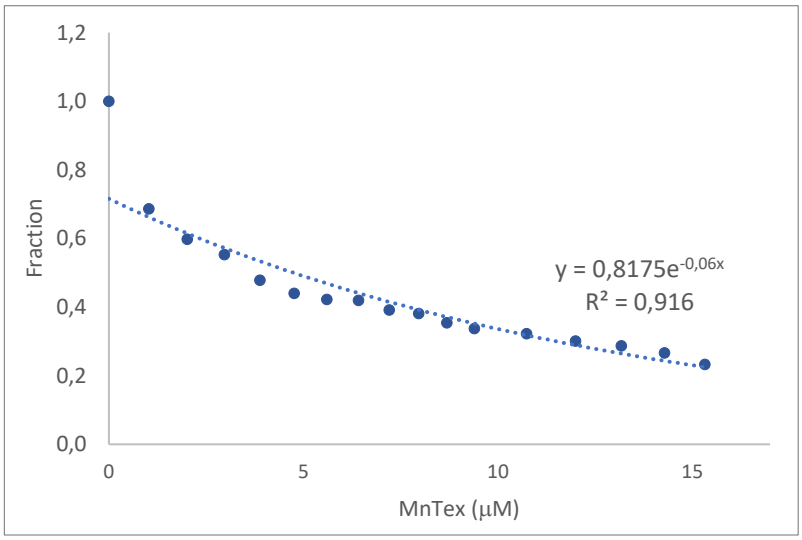

Fig. 48 *Calibration line with aggregated BSA (30 µM), Proteostat dye (1 µM) and increasing concentrations of MnTexCOOH (0 – 15 µM).*

Fraction value has been calculated from the ratio between the single fluorescence intensity ($F_{BSA+Yat+MnTex}$) and the first one from the solution without texaphyryn ($F_{BSA+Yat}$) subtracting the fluorescence intensity of the dye alone (F_{Yat}). To correct the early fluorescence intensity values, each intensity was divided by the respective fraction value.

$$Fraction = \frac{F_{BSA+Yat+MnTex} - F_{Yat}}{F_{BSA+Yat} - F_{Yat}}$$

$$Corrected\ F.Value = \frac{Initial\ F.value}{Fraction}$$

4.5.5. MnTexCOOH inhibition activity on Aβ40 aggregation

To study the inhibitory activity of the MnTexCOOH complex against amyloid aggregates formed by Aβ40 peptide a fluorescence emission kinetic study was performed, again using the fluorescent dye Yat ProteoStat.

A plate was prepared with a control solution containing only Aβ40 at a concentration of 30 μM a control solution containing only MnTexCOOH at a concentration of 10 μM, both in native buffer. Subsequently, eight solutions containing increasing concentrations of MnTexCOOH and a constant Aβ40 concentration of 30 μM were prepared, also in native buffer. The ProteoStat dye was added at a concentration of 1 μM to all control and sample solutions. The kinetics were carried out at 37 °C (the aggregation temperature of BSA) for 20 hours under agitation at 700 rpm. Once the measurement ended, the fluorescence emission value, "End point", was determined. From this value, along with those of the two control solutions, the percentage of aggregation inhibition was calculated using the above-mentioned equation. The same correction assay used for BSA was performed, another calibration curve was constructed and from his equation was possible to interpolate the fraction value. From this value it was possible to determine the correct fluorescence values, using the equations mentioned above.

Additions	MnTex (μM)	Fluorescence (AU)	Fraction
0	0	15,154	1,000
1	1,0	10,665	0,684
2	2,0	9,701	0,617
3	3,0	8,229	0,513
4	3,9	7,766	0,480
5	4,8	6,768	0,410
6	5,6	5,974	0,354
7	6,4	5,774	0,340
8	7,2	5,635	0,331
9	8,0	5,288	0,306
10	8,7	4,919	0,280
11	9,4	4,706	0,265
12	10,7	4,480	0,249
13	12,0	4,069	0,221
14	13,2	3,322	0,168
15	14,3	3,307	0,167

Tab. 23 *Spectrophotometric titration data of MnTexCOOH with aggregated Aβ and Proteostat dye.*

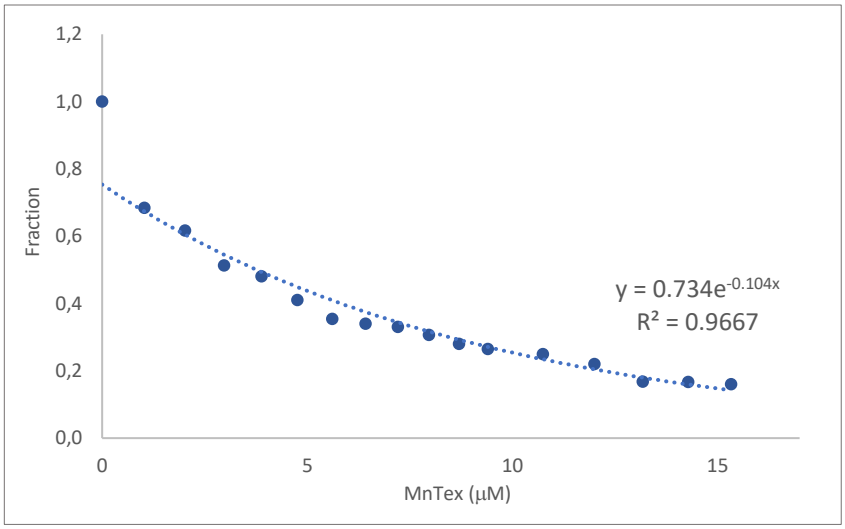

Fig. 49 *Calibration line with aggregated Aβ (30 µM), Proteostat dye (1 µM) and increasing concentrations of MnTexCOOH (0 – 15 µM).*

MnTexCOOH inhibition activity on Aβ40 aggregation – E.Coli assay

For this experiment, a batch of bacteria produced by the laboratory of the Department of Pharmacy at the University of Barcelona, stored at 4°C and induced to express the Aβ40 peptide intracellularly, was used. As a first step, a "starting medium" solution containing nutrients for the growth of E. Coli bacteria is prepared, containing:

- 5 mL Salts 10X
- 500 µL Glucose 40 %
- 100 µL $MgSO_4$ 1 M
- 100 µL $CaCl_2$ 50 mM
- MilliQ water up until 50 mL

The solution designated as "Salts 10X" contains the essential macro-elements for bacterial growth and maintains a constant pH; it is composed of Na_2HPO_4, KH_2PO_4, NH_4Cl e NaCl. Subsequently, a solution (the "ON solution") containing the frozen bacteria is prepared from the "Starting medium" and incubated overnight at 37°C with agitation at 220 rpm:

- 10 mL of Starting Medium solution
- E. Coli 1 spatula tip
- 10 µL of Kanamycin + 10 µL of Chloramphenicol

The following day, the solution containing the bacteria is divided into two separate Falcon tubes; the first (Solution 1) contains:

- 20 mL of Starting medium solution
- 20 μL of Isopropyl β-D-1-thiogalactopyranoside (IPTG)
- 20 μL of Kanamycin
- 20 μL of Chloramphenicol
- 20 μL Yat Proteostat 1 μM.

The second Falcon tube (Solution 2) contains:

- 20 mL of Starting medium solution
- 20 μL of Kanamycin
- 20 μL of Chloramphenicol
- 20 μL Yat Proteostat 1 μM.

Aliquots are prepared in Eppendorf tubes starting from Solution 1 and Solution 2 separately; increasing concentrations of MnTexCOOH are added to each tube:

- 10 μL of MnTexCOOH (in order to have different concentrations 0,5 - 2 - 5 - 15 - 30 μM)
- 790 μL of Solution 1 o 2
- 200 μL of ON solution

All the Eppendorf tubes were incubated overnight at 37 °C under moderate shaking (220 rpm). The following day, both absorbance (at 600 nm) and fluorescence intensity (at 485/590 nm) were measured for all samples using an appropriate microplate; based on the obtained values it was possible to calculate the percentage of texaphyrin's inhibition activity on the aggregation of the peptide:

$$\%\, Inhibition = 1 - \left(\frac{Fluo/Abs_{\,with\ IPTG+MnTex} - Fluo/Abs_{\,without\ IPTG+MnTex}}{Fluo/Abs_{\,with\ IPTG} - Fluo/Abs_{\,without\ IPTG}}\right) \cdot 100$$

Without IPTG:

		MnTexCOOH				
	Control	0,5 μM	2 μM	5 μM	15 μM	30 μM
Fluorescence (AU)	86921	88086	80475	72095	63602	48902
Absorbance (AU)	0,8346	0,8519	0,8847	0,8993	0,8868	0,9202
Fluo/Abs	104146,9	103399,5	90963,0	80167,9	71720,8	53142,8

With IPTG:

		MnTexCOOH				
	Control	0,5 μM	2 μM	5 μM	15 μM	30 μM
Fluorescence (AU)	157724	133768	125272	107482	90322	56525
Absorbance (AU)	0,5237	0,5596	0,5698	0,5616	0,5698	0,5765
Fluo/Abs	301172,4	239042,2	219852,6	191385,3	158515,3	98048,6
Inhib. activity	-	0,69	0,65	0,56	0,44	0,23
Inhibition %	-	**31%**	**35%**	**44%**	**56%**	**77%**

Tab. 24 *Absorbance and Fluorescence intensity of the control solutions and samples with increasing concentrations of MnTexCOOH, first set without IPTG and second set with IPTG, along with the inhibition activity percentage.*

5. Conclusions

The purpose of the study was to evaluate the antioxidant properties of the FeTCPC complex and the catalase-like activity of the MnTPCMe complex by observing their behavior and comparing it, respectively, with that of the hemin complex and bovine catalase as a reference. In the second phase of the study, the objective was to observe the inhibitory activity of the MnTexCOOH complex against amyloid aggregates.

An initial reactivity study was conducted to evaluate the pseudo-peroxidase activity of the synthesized FeTCPC complex through kinetic experiments; the complex's role as a catalyst in the hydrogen peroxide dismutation reaction was assessed, with the aim of rendering it a non-harmful species. By interpreting the results, it was possible to compare the activity of FeTCPC with that of hemin as a reference compound; it can be stated that the complex exhibits a lower affinity for the substrate than that shown by hemin, both in the case of HPA and in the case of 4-MC; a phenomenon confirmed experimentally in both cases by the value of the K_M constant, which is higher for FeTCPC than the one calculated for hemin.

Calculation of the k_{cat} constant for the FeTCPC complex with the two substrates yielded a higher value in both cases than the one calculated for hemin, indicating that FeTCPC possesses greater catalytic activity and a higher turnover number than hemin. In this case, the experiment with the 4-MC substrate yielded a higher k_{cat} constant than the experiment with HPA; this result is due to an intrinsic difference between the two substrates. 4-MC is characterized by a higher electron density than that of HPA, so it donates an electron more readily to the catalyst complex, showing a lower oxidation potential than HPA. This phenomenon results in a faster turnover rate for 4-MC in the reaction catalyzed by FeTCPC.

Subsequently, the pseudo-catalase activity of the second synthesized corrole complex, MnTPCMe, was evaluated through kinetic experiments; in this case as well, the dismutation reaction of hydrogen peroxide is catalyzed, producing water and oxygen. The reactivity study revealed that the complex exhibits catalase activity similar and equally efficient as that of the reference enzyme: bovine liver catalase.

The second section of the study has been conducted in the laboratories of the chemistry and pharmacy departments at the University of Barcelona. This part of the study focused on a manganese-texaphyrin complex, MnTexCOOH. In this phase of the work, the complex was used to inhibit the amyloid aggregation of the $A\beta_{40}$ peptide and the BSA protein; fluorescent dye Yat ProteoStat was used to monitor the various stages of aggregation.

Fluorescence studies, DLS and AFM analysis demonstrated that MnTexCOOH exhibits excellent inhibitory activity, reaching a maximum aggregation inhibition of 83% in the BSA assay and 76% in the $A\beta_{40}$ peptide assay. It has been hypothesized that the interaction between the MnTexCOOH complex and the peptide occurs when $A\beta_{40}$ is in its monomeric state; a metal-ligand bond would form with the nitrogen of the terminal amino group of the peptide chain, with the nitrogen atom donating an electron pair.

This interaction would prevent the peptide from binding to other monomers, thereby blocking the aggregation process, the formation of oligomers, and, ultimately, amyloid fibrils.
The final section of the study was conducted to observe the inhibition of $A\beta_{40}$ peptide aggregation, this time within the Gram-negative bacterium *E. coli*. A maximum inhibitory activity of 77% was achieved, indicating that the complex possesses excellent inhibitory activity. Furthermore, the results demonstrated that the complex permeated the double lipid membrane typical of Gram-negative bacteria.

It can be concluded that the FeTCPC corrole complex exhibits a higher peroxidase-like activity with the involvement of 4-MC as a substrate then HPA, overall corrole's antioxidant activity is comparable to the one of hemin. Futhermore, the MnTPCMe complex demonstrated significant catalase-like activity. Finally, the second porphyrinoid complex examined, MnTexCOOH, demonstrated high efficacy in inhibiting amyloid aggregation, proving to be a valuable compound with potential as a therapeutic agent for neurodegenerative diseases.
At the end of this study, it can be stated that both categories of porphyrin-like complexes studied represent a valid starting point for potential future studies aimed at counteracting oxidative stress and the neurotoxicity associated with amyloid aggregation.

6. References

(1) Bacchella, C.; De Caro, S.; Nicolis, S.; Monzani, E.; Dell'Acqua, S. Hemin, Copper and Amyloid-β: A Medley Involved in Alzheimer's Disease. An Interaction That Fine Regulates the Reactivity. *J. Inorg. Biochem.* **2025**, *263*, 112775. https://doi.org/10.1016/j.jinorgbio.2024.112775

(2) Kepp, K. P. Bioinorganic Chemistry of Alzheimer's Disease. *Chem. Rev.* **2012**, *112* (10), 5193–5239. https://doi.org/10.1021/cr300009x

(3) Brewster, J. T.; Thiabaud, G. D.; Harvey, P.; Zafar, H.; Reuther, J. F.; Dell'Acqua, S.; Johnson, R. M.; Root, H. D.; Metola, P.; Jasanoff, A.; Casella, L.; Sessler, J. L. Metallotexaphyrins as MRI-Active Catalytic Antioxidants for Neurodegenerative Disease: A Study on Alzheimer's Disease. *Chem* **2020**, *6* (3), 703–724. https://doi.org/10.1016/j.chempr.2019.12.016

(4) Subedi, S.; Sasidharan, S.; Nag, N.; Saudagar, P.; Tripathi, T. Amyloid Cross-Seeding: Mechanism, Implication, and Inhibition. *Molecules* **2022**, *27* (6), 1776. https://doi.org/10.3390/molecules27061776

(5) Nunan, J.; Small, D. H. Regulation of APP Cleavage by A-, B- and Γ-secretases. *FEBS Lett.* **2000**, *483* (1), 6–10. https://doi.org/10.1016/S0014-5793(00)02076-7

(6) Spies; Petra E.; Marcel M. Verbeek; Thomas van Groen. Reviewing Reasons for the Decreased CSF Abeta42 Concentration in Alzheimer Disease. *Front. Biosci.* **2012**, *17* (7).

(7) Polanco, D.; Carrancho, A.; Gracia, P.; Cremades, N. Characterisation of Amyloid Aggregation and Inhibition by Diffusion-Based Single-Molecule Fluorescence Techniques. *Biophysica* **2022**, *2* (4), 506–524. https://doi.org/10.3390/biophysica2040043

(8) Tõugu, V.; Tiiman, A.; Palumaa, P. Interactions of Zn(Ii) and Cu(Ii) Ions with Alzheimer's Amyloid-Beta Peptide. Metal Ion Binding, Contribution to Fibrillization and Toxicity. *Metallomics* **2011**, *3* (3), 250. https://doi.org/10.1039/c0mt00073f

(9) Zhang, Y.; Wang, Q.; Wen, J.; Wang, X.; Mahmood, M. H.; Ji, L.; Liu, H. DNA Binding and Oxidative Cleavage by a Water-soluble Carboxyl Manganese(III) Corrole. *Chin. J. Chem.* **2013**, *31* (10), 1321–1328. https://doi.org/10.1002/cjoc.201300488

(10) Liang, Z.-H.; Liu, H.-Y.; Zhou, R.; Zhang, Z.; Ali, A.; Han, B.-J.; Liu, Y.-J.; Xiao, X.-Y. DNA-Binding, Photocleavage, and Photodynamic Anti-Cancer Activities of Pyridyl Corroles. *J. Membr. Biol.* **2016**, *249* (4), 419–428. https://doi.org/10.1007/s00232-016-9879-0

(11) Georgiades, S. N.; Abd Karim, N. H.; Suntharalingam, K.; Vilar, R. Interaction of Metal Complexes with G-Quadruplex DNA. *Angew. Chem. Int. Ed.* **2010**, *49* (24), 4020–4034. https://doi.org/10.1002/anie.200906363

(12) Mahammed, A.; Gross, Z. The Importance of Developing Metal Complexes with Pronounced Catalase-like Activity. *Catal. Sci. Technol.* **2011**, *1* (4), 535. https://doi.org/10.1039/c1cy00063b

(13) Haber, A.; Mahammed, A.; Fuhrman, B.; Volkova, N.; Coleman, R.; Hayek, T.; Aviram, M.; Gross, Z. Amphiphilic/Bipolar Metallocorroles That Catalyze the Decomposition of Reactive Oxygen and Nitrogen Species, Rescue Lipoproteins from Oxidative Damage, and Attenuate

Atherosclerosis in Mice. *Angew. Chem. Int. Ed.* **2008**, *47* (41), 7896–7900. https://doi.org/10.1002/anie.200801149

(14) Lu, J.; Liu, H. Y.; Shi, L.; Wang, X. L.; Ying, X.; Zhang, L.; Ji, L. N.; Zang, L. Q.; Chang, C. K. DNA Cleavage Mediated by Water-Soluble Manganese Corrole. *Chin. Chem. Lett.* **2011**, *22* (1), 101–104. https://doi.org/10.1016/j.cclet.2010.09.005

(15) Fu, B.; Zhang, D.; Weng, X.; Zhang, M.; Ma, H.; Ma, Y.; Zhou, X. Cationic Metal–Corrole Complexes: Design, Synthesis, and Properties of Guanine-Quadruplex Stabilizers. *Chem. – Eur. J.* **2008**, *14* (30), 9431–9441. https://doi.org/10.1002/chem.200800835

(16) Furtmüller, P. G.; Zederbauer, M.; Jantschko, W.; Helm, J.; Bogner, M.; Jakopitsch, C.; Obinger, C. Active Site Structure and Catalytic Mechanisms of Human Peroxidases. *Arch. Biochem. Biophys.* **2006**, *445* (2), 199–213. https://doi.org/10.1016/j.abb.2005.09.017

(17) Rodríguez-López, J. N.; Gilabert, M. A.; Tudela, J.; Thorneley, R. N. F.; García-Cánovas, F. Reactivity of Horseradish Peroxidase Compound II toward Substrates: Kinetic Evidence for a Two-Step Mechanism. *Biochemistry* **2000**, *39* (43), 13201–13209. https://doi.org/10.1021/bi001150p

(18) Srinivasan, B. A Guide to the Michaelis–Menten Equation: Steady State and Beyond. *FEBS J.* **2022**, *289* (20), 6086–6098. https://doi.org/10.1111/febs.16124

(19) Lück, H. Catalase. In *Methods of Enzymatic Analysis*; Elsevier, 1965; pp 885–894. https://doi.org/10.1016/B978-0-12-395630-9.50158-4

(20) Bhattacharya, M.; Jain, N.; Mukhopadhyay, S. Insights into the Mechanism of Aggregation and Fibril Formation from Bovine Serum Albumin. *J. Phys. Chem. B* **2011**, *115* (14), 4195–4205. https://doi.org/10.1021/jp111528c

(21) Navarro, S.; Ventura, S. Fluorescent Dye ProteoStat to Detect and Discriminate Intracellular Amyloid-like Aggregates in *Escherichia Coli*. *Biotechnol. J.* **2014**, *9* (10), 1259–1266. https://doi.org/10.1002/biot.201400291

(22) Álvarez-Berbel, I.; Llabrés, S.; Domènech, Ò.; Busquets, M. A.; Fernàndez-Busquets, X.; Arce, E. M.; Gavín, R.; Del Río, J. A.; Muñoz-Torrero, D.; Luque, F. J.; Sabate, R.; Espargaró, A. YAT2150: Overcoming Limitations of Traditional Amyloid Dyes in Aggregation Studies. *Bioorg. Med. Chem.* **2025**, *123*, 118163. https://doi.org/10.1016/j.bmc.2025.118163

(23) Kovalska, V.; Losytskyy, M.; Chernii, V.; Volkova, K.; Tretyakova, I.; Cherepanov, V.; Yarmoluk, S.; Volkov, S. Studies of Anti-Fibrillogenic Activity of Phthalocyanines of Zirconium Containing out-of-Plane Ligands. *Bioorg. Med. Chem.* **2012**, *20* (1), 330–334. https://doi.org/10.1016/j.bmc.2011.10.083

(24) Aykul, S.; Martinez-Hackert, E. Determination of Half-Maximal Inhibitory Concentration Using Biosensor-Based Protein Interaction Analysis. *Anal. Biochem.* **2016**, *508*, 97–103. https://doi.org/10.1016/j.ab.2016.06.025

(25) *Textbook on Cloning, Expression and Purification of Recombinant Proteins*; Bose, K., Ed.; Springer Nature Singapore: Singapore, 2022. https://doi.org/10.1007/978-981-16-4987-5

(26) Zhao, Y.; Qi, S.; Niu, Z.; Peng, Y.; Shan, C.; Verma, G.; Wojtas, L.; Zhang, Z.; Zhang, B.; Feng, Y.; Chen, Y.-S.; Ma, S. Robust Corrole-Based Metal–Organic Frameworks with Rare 9-Connected Zr/Hf-Oxo Clusters. *J. Am. Chem. Soc.* **2019**, *141* (36), 14443–14450. https://doi.org/10.1021/jacs.9b07700

(27) Dell'Acqua, S.; Pirota, V.; Monzani, E.; Camponeschi, F.; De Ricco, R.; Valensin, D.; Casella, L. Copper(I) Forms a Redox-Stable 1:2 Complex with α-Synuclein N-Terminal Peptide in a Membrane-Like Environment. *Inorg. Chem.* **2016**, *55* (12), 6100–6106. https://doi.org/10.1021/acs.inorgchem.6b00641